Heliyon 10 (2024) e24605

Contents lists available at ScienceDirect

Heliyon

journal homepage: www.cell.com/heliyon

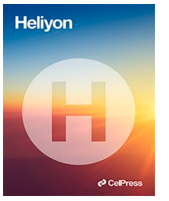

Research article

Interactions of ferulic acid and ferulic acid methyl ester with endogenous proteins: Determination using the multi-methods

Ying Yang [a,1], Shuqin Wang [a,1], Xingyan Liu [a], Wenbin Zhang [c], Wenhua Tong [a,b,*,1], Huibo Luo [a,b], Liming Zhao [d,**]

[a] School of Biological Engineering, Sichuan University of Science and Engineering, Yibin, 644000, China
[b] Key Laboratory of Brewing Biotechnology and Application, Yibin, 644000, China
[c] Guangdong Provincial Key Laboratory of Protein Function and Regulation in Agricultural Organisms, College of Life Sciences, South China Agricultural University, Guangzhou, 510000, China
[d] East China University of Science and Technology, Shanghai, 200000, China

ARTICLE INFO

Keywords:
Ferulic acid
Ferulic acid methyl ester
Human serum albumin
Lysozyme
Molecular dynamics simulations
Resonance light scattering

ABSTRACT

Ferulic acid (FA) and ferulic acid methyl ester (FAM) are important phenolic compounds in Baijiu. In this study, the interaction of FA and FAM with human serum albumin (HSA) and lysozyme (LZM) was investigated using multispectral methods and molecular dynamics simulation. FA and FAM could interact with HSA and LZM, changing the conformation and hydrophilicity of the protein. The quenching mechanisms of FA-HSA, FA-LZM, FAM-HSA, and FAM-LZM were all static-quenching. In the FA-HSA, FAM-HSA, and FA-LZM systems, the interaction forces were mainly hydrophobic interactions and hydrogen bonding. In the FAM-LZM system, the interaction forces were mainly hydrophobic interactions, hydrogen bonding, and van der Waals force. Common metal ions such as K^+, Ca^{2+}, Cu^{2+}, Mg^{2+}, and Mn^{2+} could affect the binding ability of FA and FAM to HSA and LZM. Moreover, FA and FAM could increase the stability of HSA and LZM, and the protein bound to FA/FAM was more stable than the free protein. FA and FAM had varying degrees of impact on the physiological activities of HSA and LZM. This study provides relevant information on the interactions and metabolic mechanisms of FA and its derivatives with endogenous proteins.

1. Introduction

Ferulic acid (FA) is a phenolic acid that is widely found in plants and is also the main active substance of Angelica and rice bran polyphenols; it is used to extract fatty acids [1]. FA constitutes 0.5 %–2 % (1.4 % dry weight) of the cell walls of cereals and various edible plants (pineapple, banana, spinach, and beetroot), mainly in the form of trans isomers and esterification with specific polysaccharides. FA can promote angiogenesis of vascular endothelial cells under normoxic conditions and has antithrombotic and antioxidant effects. Moreover, it is used in the prevention and treatment of coronary artery disease [2]. Ferulic acid methyl ester (FAM), a

* Corresponding author. School of Biological Engineering, Sichuan University of Science and Engineering, Yibin, 644000, China.tongwh@suse.edu.cn
** Corresponding author.
E-mail address: zhaoliming@ecust.edu.cn (L. Zhao).
[1] Ying Yang, Shuqin Wang and Wenhua Tong contributes equally to this work.

https://doi.org/10.1016/j.heliyon.2024.e24605
Received 20 July 2023; Received in revised form 9 January 2024; Accepted 10 January 2024
Available online 13 January 2024

derivatives of FA, is a potent antibacterial component in plants that reduces oxidation [3]. FAM exerts antitumor activity in liver cancer and breast cancer, inhibits thrombosis, and has antioxidant and anti-inflammatory functions. Studies have shown that FA and FAM are the important bioactive compounds of Baijiu [4]. Besides, they have good application value and exhibit potential in the food industry.

Human serum albumin (HSA) is a natural transport carrier in the blood that can reversibly and noncovalently bind to numerous endogenous (metabolites, etc.) and exogenous (drugs, etc.) substances, thereby performing physiological functions such as storage, transport, and protection [5–7]. Studies show that HSA can be preferentially ingested by tumor or inflammatory tissues and that it penetrates tumor-like or inflammatory sites better than it does healthy tissues [8]. Lysozyme (LZM), also known as cytosolic enzyme or *N*-acetyl cytosolic glycan hydrolase, is a powerful bactericidal substance that was first found in the nasal mucus by the British bacteriologist Fleming in 1922 [9]. It is a small alkaline protein widely present in tears, saliva, plasma, and milk of humans and other mammals, as well as in egg whites of birds and poultry [10]. LZM has antibacterial, antiviral, antitumor and immune-enhancing effects. HSA and LZM are present in numerous sources and often used as model proteins to study the interactions of small drug molecules with proteins, providing a basis to study their distribution, metabolism, and efficacy of drugs in the body [11–14]. Moreover, HSA and LZM have been widely used in the pharmaceutical and food industries [15–17].

To date, there are no reports on the use of spectral methods to study the binding effects of phenolic acids and their derivatives with HSA/LZM. In this study, we focused on the binding mechanisms of FA and FAM to HSA and LZM, respectively, under simulated physiological conditions using multi-methods. The forces and conformational changes of FA and FAM interacting with HSA and LZM were also studied. Furthermore, the effects of common metal ions binding to these four systems were explored. This paper has positive significance for understanding the binding, transport, and metabolism of phenolic acids in the process of blood circulation. At the same time, the key data of phenolic acid compounds in the metabolic process in vivo were provided, which provided important parameters for the study of the health effects of such functional factors in food.

2. Experimental

2.1. Reagents

HSA (A1653, ≥96 %, agarose gel electrophoresis) was purchased from Sigma-Aldrich (Shanghai, China). LZM (A610308-000, Molecular Biology Grade, Potency≥20000U/mg) procured from Shenggong Bioengineering (Shanghai, China). HSA and LZM were dissolved in Tris-HCl (D885211; 0.05 mol L^{-1}, pH = 7.40) buffer to obtain 1.58×10^{-4} mol L^{-1} LZM and 1.00×10^{-4} mol L^{-1} HSA. FA (F10370; 99 %), FAM (F189084; 99 %), and dimethyl sulfoxide (DMSO; D806645; 99 %) were purchased from Shanghai Aladdin Biochemical Technology Co., Ltd (Shanghai, China). FA and FAM were dissolved in DMSO to obtain solutions with concentrations of 2.50×10^{-4} mol L^{-1} and 1.875×10^{-3} mol L^{-1}, respectively.

2.2. Apparatus

Fluorescence spectrophotometer (PerkinElmer, LS55, USA), Aarhus American electronic balance (Aarhus, CP213, USA), ultraviolet (UV)-visible spectrophotometer (Shimadzu, UV19001, Japan), circular dichroism (CD; Applied Photophysics Ltd, Chirascan, UK), and a microplate reader (Thermo Fisher, Multiskan FC, Shanghai) were some of the equipment used in this study.

2.3. Methods

2.3.1. Fluorescence emission spectrum

A certain volume of FA or FAM (2.50×10^{-4} mol L^{-1}) was added successively to the HSA solution (1.00×10^{-4} mol L^{-1}, volume 2.5 mL) to yield FA and FAM at concentrations of 1.00, 2.00, 3.00, 4.00, 5.00, 6.00, 7.00, 8.00, and 9.00 ($\times 10^{-6}$ mol L^{-1}). The excitation (EX) wavelength was 292 nm, and the emission (EM) wavelength was recorded from 300 to 600 nm. The slit widths of the EX and EM wavelengths were set at 15 nm. Fluorescence emission spectra were measured at 4 different temperatures (291, 298, 304, and 310 K).

A certain volume of FA/FAM (1.875×10^{-3} mol L^{-1}) was added successively to the LZM solution (1.58×10^{-4} mol L^{-1}, volume 2.5 mL). The FA/FAM concentrations were 7.50, 15.00, 22.50, 30.00, 37.50, 45.00, 52.50, 60.00, and 67.50 ($\times 10^{-6}$ mol L^{-1}). The EX wavelength was set to 292 nm, and the EM wavelength was recorded from 300 to 600 nm. The slit widths for the EX and EM wavelengths were set at 15 nm. Fluorescence emission spectra were measured at 4 different temperatures (291, 297, 303, and 310 K).

2.3.2. Molecular docking and molecular dynamic simulations

2.3.2.1. Molecular docking. FA/FAM-protein interactions were analyzed using AutoDock software. The crystal structure of HSA (Protein Data Bank [PDB] ID: 6YG9) and LZM (PDB ID: 1REX) were taken from the RCSB PDB (http://www.rcsb.org/pdb). The structures of FA and FAM were downloaded from the PubChem database (https://pubchem.ncbi.nlm.nih.gov/). The water molecules in HSA and LZM were removed before molecular docking. FA/FAM and proteins were hydrogenated and charged to minimize energy using AutoDock Tools and saved as an alternative in the pdbqt format. The PyRx software (https://pyrx.sourceforge.io/) tool AutoDock Vina was then used for blind docking strategy. During docking, HSA and LZM were used as the receptors and FA and FAM as the

ligands. In this study, the centers of the grid boxes of HSA and LZM were set at points 29.130, 0.157, and 18.966, and at points 13.358, 14.691, and 28.231, respectively; the grid box sizes were 86.281 × 47.909 × 86.665 and 36.395 × 42.272 × 35.856, respectively; and the grid point spacing was 0.376 Å and 0.317 Å, respectively. The number of docking runs was 50 times. The results were visualized using PyMol (https://pymol.org/2/), wherein the affinity (kcal/mol) value represents the binding ability of the two. The lower the binding ability, the more stable the ligand and receptor binding. 2D plots were visualized and analyzed using Discovery Studio 2020 Client (https://discover.3ds.com/discovery-studio-visualizer-download).

2.3.2.2. Molecular dynamics simulation. Molecular dynamics simulation was performed for the complex using Gromacs 2022 and AMBER 19 force field. Firstly, a cubic box was placed around all atoms (distance is 10 Å) according to the periodic boundary condition. TIP3P water molecules with a density of 0.10 g/mL were used to solvate the system. The simulated temperature was controlled at 298 K for HSA and 297 K for LZM and the pressure was controlled at 1 bar. Long range electrostatic interactions were calculated using the particle mesh Ewald method with an 8 Å cutoff. The time step was 2 fs, and simulation snapshots were saved every 25 ps during the simulation. The simulation for each system was performed for 200 ns. Lastly, analysis of the complex root mean square deviation (RMSD) and protein root mean square fluctuation (RMSF) were obtained from the molecular dynamics trajectories, whereas analysis of the binding energy was conducted using gmx_MMPBSA.

2.3.3. Effects of FA and FAM on the physiological functions of HSA and LZM

2.3.3.1. Determination of esterase activity. HSA and LZM were mixed with different concentrations of FA and FAM for 30 min, and pNPA was added to measure the absorbance of the reaction product at 400 nm.

2.3.3.2. Determination of free radical scavenging ability. HSA and LZM were mixed with different concentrations of FA and FAM at room temperature for 30 min, followed by the addition of Ellman reagent. The absorbance of the reaction product was measured at 412 nm.

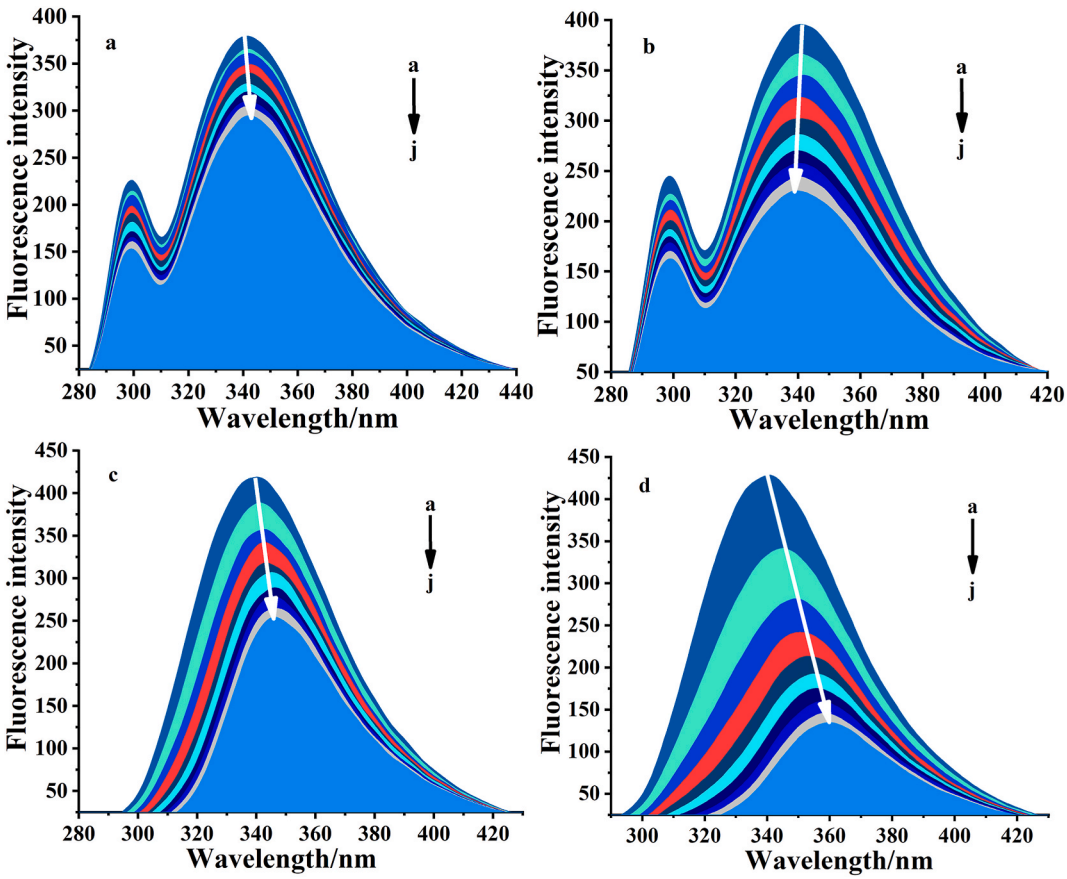

Fig. 1. Fluorescence quenching spectrum of FA-HSA(a), FAM-HSA(b), FA-LZM(c) and FAM-LZM(d). $C_{HSA} = 1.00 \times 10^{-4}$ mol L^{-1}, T = 298 K. C_{FA} (a-j) = C_{FAM} (a–j) = 1.00, 2.00, 3.00, 4.00, 5.00, 6.00, 7.00, 8.00, 9.00 ($\times 10^{-6}$ moL•L^{-1}. $C_{LZM} = 1.58 \times 10^{-4}$ moL•L^{-1}, T = 297 K, C_{FA} (a–j) = C_{FAM} (a–j) = 7.50, 15.00, 22.50, 30.00, 37.50, 45.00, 52.50, 60.00, 67.50 ($\times 10^{-6}$ moL•L^{-1}).

2.3.4. Resonance light scattering (RLS)

The solution treatment method and concentration gradient were the same as that described in Section 2.3.1. The RLS spectrum of HSA in the wavelength range of 220–700 nm was determined under the condition of $\lambda_{ex} = \lambda_{em}$.

2.3.5. Data processing

The inner-filter effect should be considered as it is a factor that can decrease fluorescence intensity. The inner filter effect can be corrected using the following equation when the absorbance does not exceed 0.3 [18]:

$$F_{cor} = F_{obs} \times e^{\frac{A_{ex} + A_{em}}{2}}$$

where F_{cor} and F_{obs} are the corrected and observed fluorescence intensities, respectively, and A_{ex} and Aem are the absorption of the system at the Ex and Em wavelengths, respectively. The fluorescence data used in this paper were always adjusted.

3. Results and discussion

3.1. Fluorescence quenching constant and quenching mechanism

As HSA and LZM contain amino acid residues such as tyrosine (Tyr), tryptophan (Trp), and phenylalanine (Phe), the addition of small molecules caused HSA and LZM to produce strong endogenous fluorescence and fluorescence quenching [19,20]. With the addition of FA and FAM, the fluorescence intensity of HSA and LZM gradually decreased (Fig. 1), indicating the interactions of FA and FAM with HSA and LZM [21]. In addition, the maximum fluorescence EM wavelengths of FA-LZM, FAM-LZM, and FA-HSA systems exhibited a certain degree of red shift, mainly caused by the reduction of water content and changes in hydrogen bonds in the system. The maximum fluorescence EM wavelength of FAM-HSA underwent a blue shift, indicating that the combination of FAM and HSA changed the microenvironment near HSA and enhanced hydrophobicity.

Fluorescence quenching refers to a the decrease in the fluorescence intensity or quantum yield of fluorescence [22]. The mechanism of fluorescence quenching mainly includes static quenching, dynamic quenching, and nonradiation energy transfer [23]. The

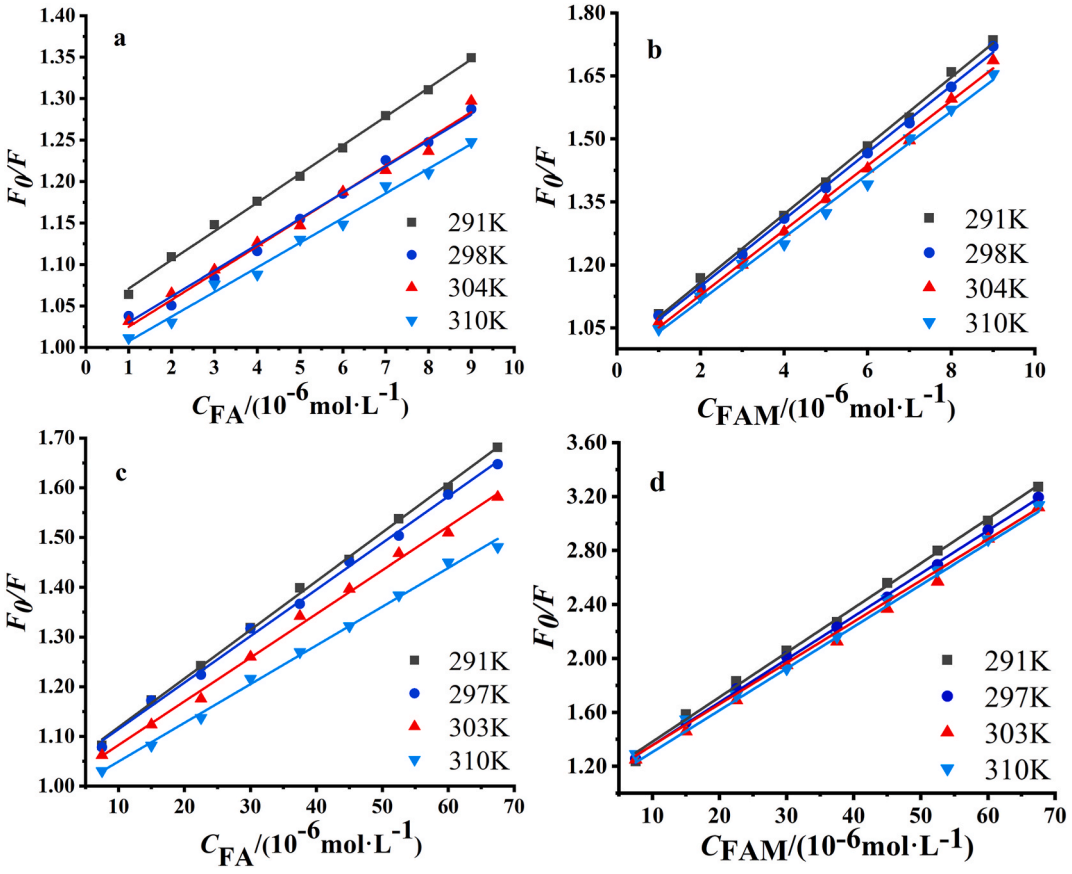

Fig. 2. Stern-Volmer curve of FA-HSA(a), FAM-HSA(b), FA-LZM(c) and FAM-LZM(d).

Stern-Volmer equation (1) [24] was used to calculate the quenching mechanism between FA and FAM, and HSA and LZM:

$$\frac{F_0}{F} = 1 + K_{sv}[Q] = 1 + K_q\tau_0[Q] \quad (1)$$

where, F and F_0 are the fluorescence intensity of the quenchers (HSA, LZM) in the presence and absence of the quenchers FA and FAM, respectively; K_{SV} and k_q are the Stern-Volmer quenching constant and bimolecular quenching process rate constant, respectively; [Q] is the concentration of FA and FAM; and τ_0 is the average life of HSA and LZM in the absence of FA and FAM (about 10^{-8} s). The Stern-Volmer diagram is derived from equation (1) as shown in Fig. 2, and the K_{SV} and k_q values are shown in Table 1.

K_{SV} is the rate constant for the interaction of a fluorescent molecule with a quencher in solution, and can be used to quantify the intensity and rate of the interaction of a fluorescent molecule with a quencher [25]. The K_{sv} values of the Stern-Volmer curves of the 4 systems decreased with increasing temperature, indicating that the quenching mechanism of the 4 systems is static quenching [26]. Moreover, the k_q value is far greater than the maximum diffusion collision quenching constant of various quenching agents on biological macromolecules (2.0×10^{10} L mol^{-1} s^{-1}); thus, it could be inferred that the fluorescence quenching of FA and FAM on HSA/LZM was a static quenching process caused by the formation of a new ground-state complexes of FA and FAM with HSA and LZM [27]. In the ground state, FA and FAM form a nonluminous ground state complex with HSA and LZM, which results in a decrease in the fluorescence of HSA and LZM and a change in the molecular structure [28].

3.2. UV–vis spectroscopy

UV–Vis spectroscopy is a commonly method for the analysis of the conformational changes in proteins [29]. Among the amino acids that make up proteins, except for the aromatic amino acids Tyr, Phe, Trp and the sulfur-containing amino acids, the other amino acids do not absorb in the UV spectrum in the 230–310 nm range [30]. A strong absorption peak of peptide bonds is generally observed at 210 nm, and a strong absorption peak of conjugated double bonds between Tyr and Trp residues is usually seen at 280 nm [31]. The UV–vis absorption spectra of HSA and LZM in the presence of different concentrations of FA and FAM are shown in Fig. 3. The light absorption values of HSA and LZM were gradually enhanced with increasing concentrations of FA and FAM, indicating that FA and FAM could change the secondary structure of HSA and LZM. In addition, with an increase in FA concentration, the maximum absorption peaks of HSA did not shift significantly (Fig. 3a), and the maximum absorption peak of LZM underwent a red shift (Fig. 3c). With an increase in the concentration of FAM, the maximum absorption peaks of HSA and LZM underwent a red shift (Fig. 3b and d). These results indicated that the molecules of the 4 systems in the excited state reacted to form ground state complexes [32]. It was further confirmed that the fluorescence quenching mechanism was the static quenching caused by the formation of the nonluminous ground state complex [33]. The absorption peak at 280 nm also showed a slight decrease, indicating that the binding process belongs to static quenching, which was consistent with the results from fluorescence experiments [34].

3.3. Analysis of binding effects

3.3.1. Binding constant, binding sites, and determination of force type

The relationship between fluorescence intensity and quenching agent concentration can be described using equation (2) [35]. The thermodynamic parameters of the FA/FAM-HSA and FA/FAM-LZM systems were calculated using van't Hoff equations (3)–(5) [36].

$$\log\frac{(F_0 - F)}{F} = \log K_a + n\log[Q] \quad (2)$$

Table 1
The quenching constants of HSA and LZM by FA and FAM at four different temperatures.

	T/K	K_{sv}/(L • mol^{-1})	K_q/(L • mol^{-1} • s^{-1})	R
FA-HSA	291 K	3.4533×10^4	3.4533×10^{12}	0.9943
	298 K	3.2350×10^4	3.2350×10^{12}	0.9923
	304 K	3.1289×10^4	3.1289×10^{12}	0.9906
	310 K	2.9725×10^4	2.9725×10^{12}	0.9977
FAM-HSA	291 K	8.1498×10^4	8.1498×10^{12}	0.9982
	298 K	7.9617×10^4	7.9617×10^{12}	0.9988
	304 K	7.7114×10^4	7.7114×10^{12}	0.9973
	310 K	7.5060×10^4	7.5060×10^{12}	0.9949
FA-LZM	291 K	9.7940×10^3	9.7940×10^{11}	0.9987
	297 K	9.3610×10^3	9.3610×10^{11}	0.9972
	303 K	8.7930×10^3	8.7930×10^{11}	0.9962
	310 K	7.7900×10^3	7.7900×10^{11}	0.9966
FAM-LZM	291 K	3.3067×10^4	3.3067×10^{12}	0.9977
	297 K	3.1829×10^4	3.1829×10^{12}	0.9994
	303 K	3.0982×10^4	3.0982×10^{12}	0.9977
	310 K	3.0554×10^4	3.0554×10^{12}	0.9983

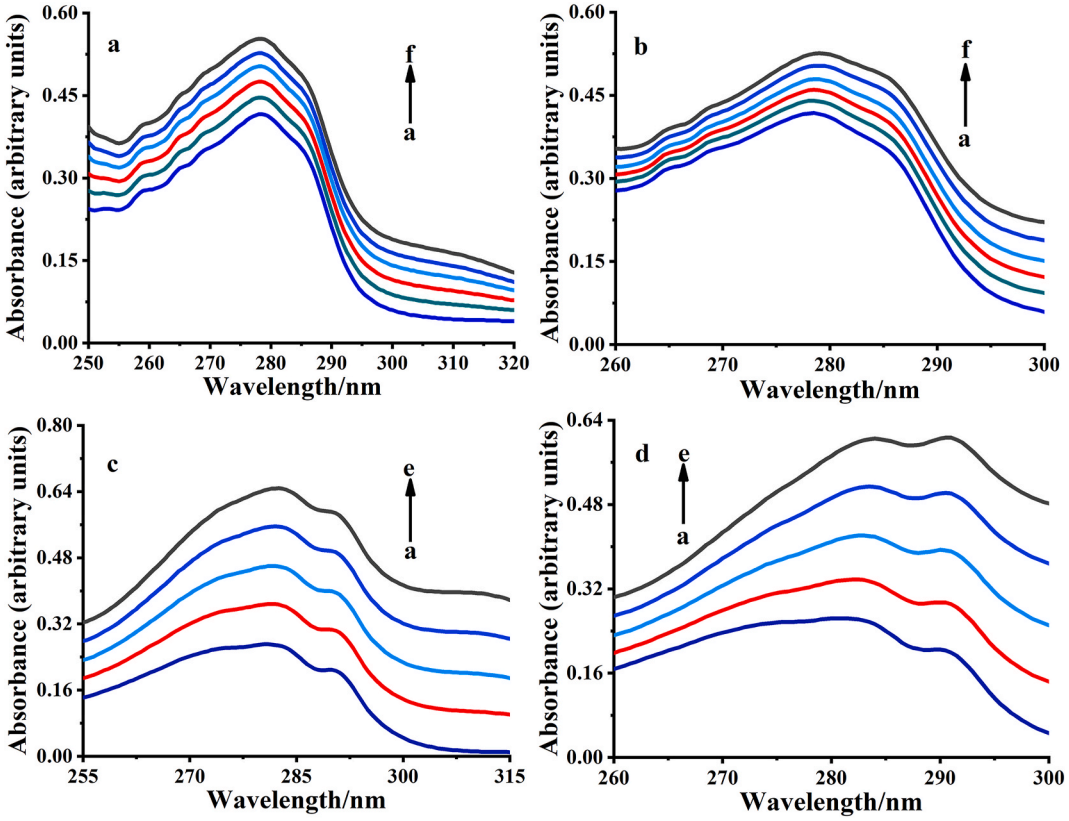

Fig. 3. UV–Vis absorption spectrum of FA-HSA(a), FAM-HSA(b), FA-LZM(c) and FAM-LZM(d).

$$\ln K_a = -\frac{\Delta H}{RT} + \frac{\Delta S}{R} \tag{3}$$

$$\Delta G = -RT \ln K_a \tag{4}$$

$$\Delta S = \frac{\Delta H - \Delta G}{T} \tag{5}$$

where, K_a is the binding constant that reflects the strength of the interaction of proteins acting with small molecules at the corresponding temperatures [37]; n is the number of binding sites; [Q] is the concentration of FA or FAM; T is the temperature; and R is the gas constant. The double logarithmic regression curve obtained from equation (2) is shown in Fig. 4. At the 4 temperatures, the double-logarithmic curve showed a good linear relationship. The binding constants were large, indicating that a relatively stable complex was formed between FA and FAM and the proteins, and that the small molecules had a strong binding effect with the two proteins. At different temperatures, the binding constants, number of binding sites, and thermodynamic parameters were calculated, and the results are shown in Table 2. FA-HSA, FAM-HSA, and FA-LZM showed the strongest binding ability at 310 K, but FAM-LZM showed the strongest binding ability at 291 K. This may be related to the structure of FAM and its binding mode with LZM. Moreover, the binding activity of FA to protein was stronger than that of FAM to protein. There are 4 possible noncovalent interactions in the protein interactions of small molecules, namely, hydrophobic interactions, electrostatic interactions, van der Waals forces, and hydrogen bond interactions [38]. Of the thermodynamic parameters, $\Delta G < 0$ indicates that the binding process is spontaneous. In the FA-HSA, FAM-HSA, and FA-LZM systems, ΔH and ΔS were positive, indicating mainly hydrophobic interaction. In the FAM-LZM system, both ΔH and ΔS were negative, indicating that the main binding force between FAM and LZM was van der Waals force and hydrogen bonding interactions [33].

3.3.2. Calculation of the binding distance

Overlap of the fluorescence emission spectra of HSA and LZM and the absorption spectra of FA and FAM are shown in Fig. 5. According to Förster's nonradioactive energy transfer theory, the energy transfer efficiency (E) and binding distance (r) between HSA, LZM, and FA/FAM can be calculated using equation (6):

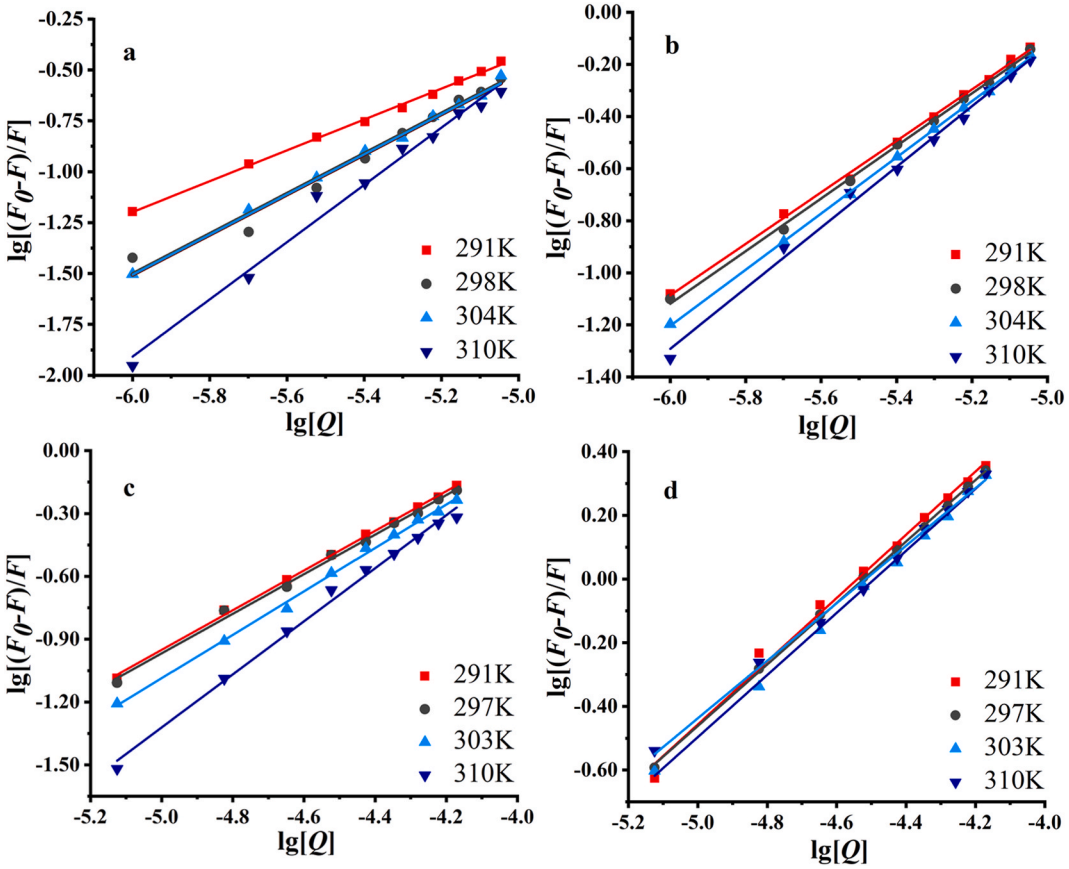

Fig. 4. Double logarithmic curve of FA-HSA(a), FAM-HSA(b), FA-LZM(c) and FAM-LZM(d).

Table 2
Binding constants, number of binding sites and thermodynamic parameters of FA-HSA, FAM-HSA, FA-LZM, and FAM-LZM.

	T/K	K_a/(L • mol^{-1})	n	R	ΔH/(kJ • mol^{-1})	ΔG/(kJ • mol^{-1})	ΔS/(J • mol • K^{-1})
FA-HSA	291 K	$2.2460 \times 10^3 \pm 1.1887$	0.7582	0.9976	258.68	−18.67	950.12
	298 K	$2.5668 \times 10^4 \pm 2.0417$	0.9857	0.9767		−25.15	
	304 K	$2.6199 \times 10^4 \pm 1.2817$	0.9860	0.9971		−25.71	
	310 K	$3.3713 \times 10^6 \pm 2.2120$	1.4059	0.9857		−38.74	
FAM-HSA	291 K	$6.9791 \times 10^4 \pm 1.2137$	0.9884	0.9982	77.58	−26.98	357.39
	298 K	$8.7256 \times 10^4 \pm 1.1863$	1.0099	0.9987		−28.19	
	304 K	$1.8513 \times 10^5 \pm 1.1169$	1.0785	0.9995		−30.66	
	310 K	$4.9567 \times 10^5 \pm 1.4838$	1.1645	0.9948		−33.80	
FA-LZM	291 K	$6.0900 \times 10^3 \pm 1.1524$	0.9471	0.9985	111.27	−21.08	450.45
	297 K	$5.7030 \times 10^3 \pm 1.2635$	0.9448	0.9960		−21.36	
	303 K	$1.2506 \times 10^4 \pm 1.2393$	1.0367	0.9972		−23.77	
	310 K	$1.0287 \times 10^5 \pm 1.4692$	1.2668	0.9940		−29.75	
FAM-LZM	291 K	$3.2350 \times 10^4 \pm 1.3925$	0.9932	0.9928	−35.28	−25.12	−34.62
	297 K	$2.3285 \times 10^4 \pm 1.0962$	0.9655	0.9994		−24.83	
	303 K	$2.3978 \times 10^4 \pm 1.1668$	0.9751	0.9983		−25.41	
	310 K	$1.2036 \times 10^4 \pm 1.2266$	0.9034	0.9967		−24.22	

$$E = 1 - \frac{F}{F_0} = \frac{R_0^6}{R_0^6 + r^6} \tag{6}$$

where, F is the fluorescence intensity when there is a quenching agent in HSA/LZM; F_0 is the fluorescence intensity when there is no quenching agent in HSA/LZM; and R_0 is the critical distance when the transfer efficiency is 50 %. R_0 is calculated using formula (7) [39]:

$$R_0^6 = 8.8 \times 10^{-25} K^2 \Phi N^{-4} J \tag{7}$$

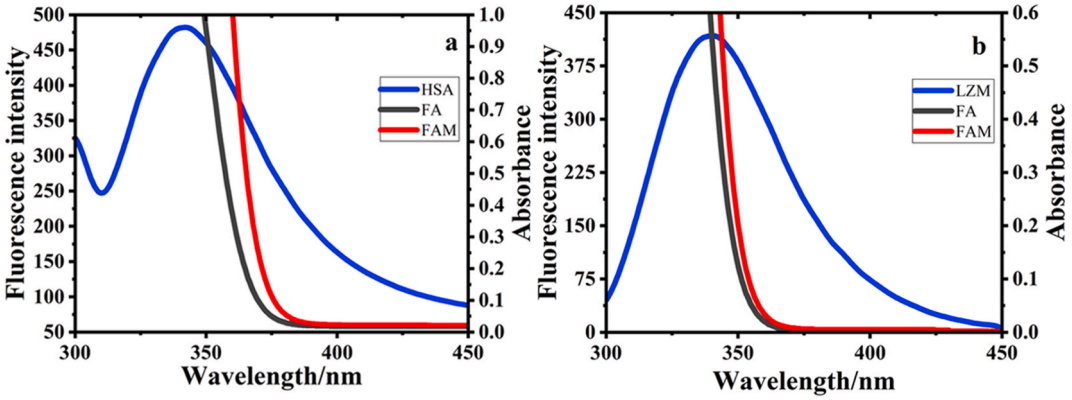

Fig. 5. Overlaps of UV–vis absorption spectrum of FA/FAM and fluorescence emission spectrum of HSA at 298 K(a), Superimposition of absorption spectrum of FA/FAM and fluorescence emission spectrum of LZM at 297 K(b).

where, K^2 is the spatial orientation factor of the dipole; N is the refractive index of the medium; φ is the quantum yield of the donor; and J is the effect of the overlap of the donor's emission spectrum and the receptor's absorption spectrum. K2 = 2/3, N = 1.336, φ = 0.118 [40]. J is calculated using equation (8) [41]:

$$J = \frac{\sum F(\lambda)\varepsilon(\lambda)\lambda^4 \Delta\lambda}{\sum F(\lambda)\Delta\lambda} \tag{8}$$

In formula (8), F (λ) is the fluorescence intensity of the protein at wavelength λ, and ε (λ) is the molar absorption coefficient of small molecules at λ. The results obtained from the above formula are shown in Table 3, indicating that nonradiation energy is transferred from FA and FAM to HSA and LZM during the whole process, which is also a reason for the fluorescence quenching of HSA and LZM [42]. Fig. 5 shows the overlapping curves of the 4 systems and indicates sufficient overlap in the absorption spectrum of the 4 systems. The binding distance (r) of the four systems is < 7 nm, and $0.5\,R_0 < r < 1.5\,R_0$, indicating nonradiative energy transfer in the 4 systems, which causes protein fluorescence quenching [43]. At the same time, the binding distance between FA and 2 proteins was less than that between FAM and 2 proteins, and FA binds more tightly to the 2 proteins with more overlapping parts.

3.4. Synchronous fluorescence spectrum

The maximum EM wavelength of a protein is related to the polarity of its environment; thus, changes in protein conformation can be determined by changes in the EM wavelength [44]. Endogenous fluorescence in HSA and LZM is mainly affected by Tyr and Trp residues. The EX and EM wavelengths Δλ were set to 15 nm and 50 nm, respectively. Fig. 6 shows the synchronous fluorescence spectrum of HSA and LZM in the presence of FA and FAM. An increase in the concentration of FA and FAM led to a decrease in the intensity of protein fluorescence. When Δλ was 15 nm, the maximum EM wavelength of fluorescence of FA-HSA was unchanged (Fig. 6a). When Δλ was 50 nm, the fluorescence EM wavelength changed from 294 nm to 293.5 nm (Fig. 6b), and the fluorescence emission peak of Trp residue showed a blue shift, indicating a change in the conformation of HSA at 50 nm. In the FAM-HSA system, when Δλ was 15 nm and 50 nm, the wavelength of the maximum fluorescence emission peak of HSA blue shifted by 0.5 nm (Fig. 6c and d), and the fluorescence EM peaks of Trp and Tyr exhibited a blue shift. The maximum fluorescence EM peak of HSA was blue shifted by FA and FAM, indicating an increase in the hydrophobicity of the microenvironment. As the degree of stretch of the peptide chain might have weakened, the structure of HSA became more compact [45]. In the FA-LZM system, the fluorescence EM peaks ranged from 302 nm to 302.5 nm and from 295 nm to 292.5 nm when Δλ was 15 nm and 50 nm, respectively (Fig. 6e and f). Therefore, the system exhibited a red shift at Δλ of 15 nm and a blue shift at Δλ of 50 nm. The red shift at Δλ of 15 nm was more pronounced than the blue shift at Δλ of 50 nm. In the FAM-LZM system, when Δλ was 15 nm and 50 nm, the fluorescence EM peak ranged from 302 nm to 300.5 nm and from 295 nm to 295.5 nm, respectively, and the system exhibited a blue shift at Δλ of 15 nm and a red shift at Δλ of 50 nm (Fig. 6g and h). The blue shift at Δλ of 15 nm was more pronounced than the red shift at Δλ of 50 nm. The maximum fluorescence EM peak of LZM was significantly red shifted by FA and FAM, and the EM wavelength was red shifted. These findings indicated an increase

Table 3
Relevant parameters of energy transfer process between HSA, LZM and FA, FAM molecules.

	J ($cm^3 \cdot mol^{-1} \cdot L) \cdot 10^{-13}$	E	R_0 (nm)	r (nm)
FA-HSA	2.06	0.2232	3.79	4.67
FAM-HSA	5.44	0.4188	4.46	4.71
FA-LZM	3.58	0.3930	4.16	4.47
FAM-LZM	5.02	0.3129	4.40	5.02

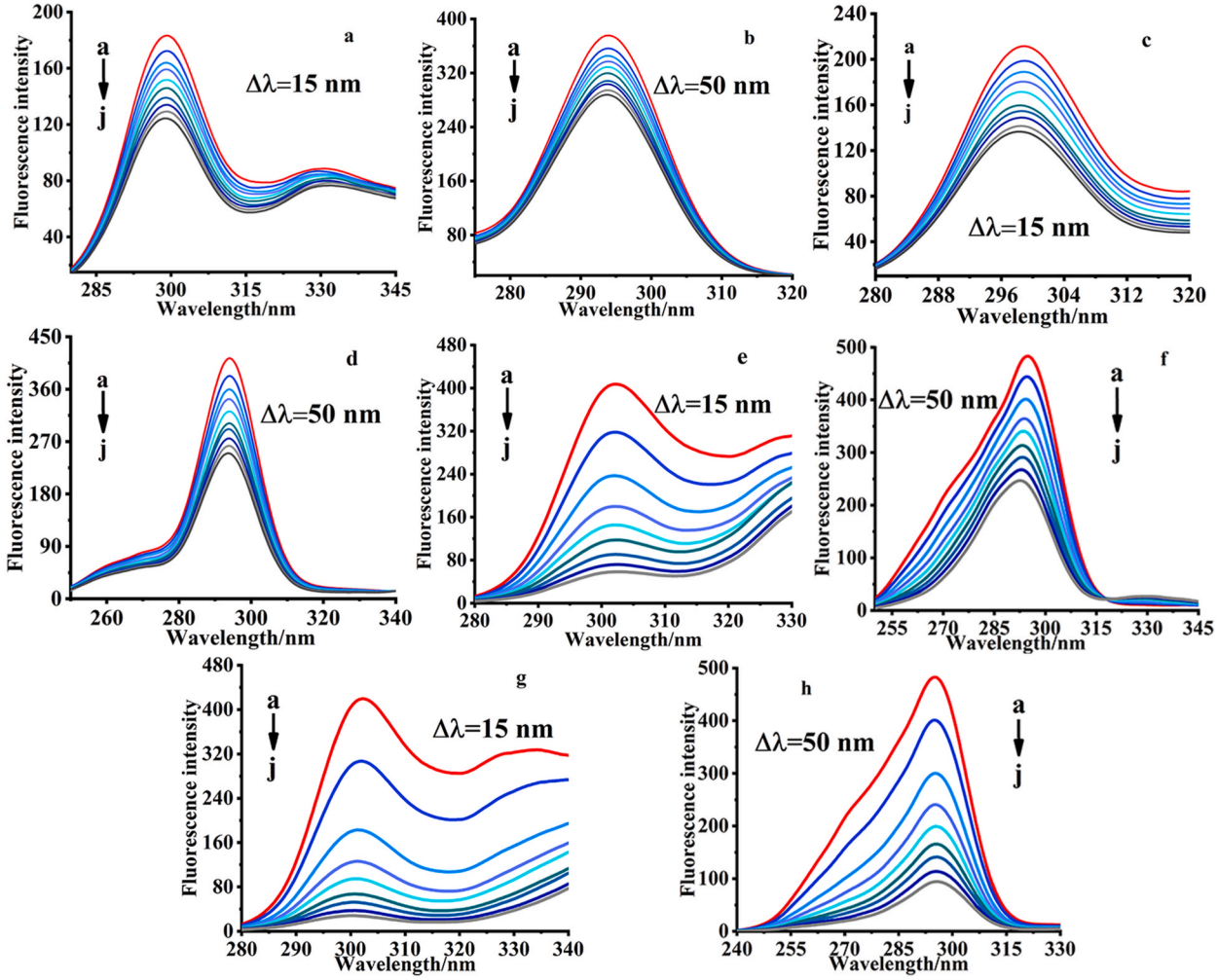

Fig. 6. Synchronous fluorescence spectrum of FA-HSA (a, b) and FAM-HSA (c, d). ($C_{HSA} = 1.00 \times 10^{-5}$ moL•L^{-1}, T = 298 K, C_{FA} (a-j) = C_{FAM}(a-j) = 1.00, 2.00, 3.00, 4.00, 5.00, 6.00, 7.00, 8.00, 9.00 ($\times 10^{-6}$ moL•L^{-1})). Synchronous fluorescence spectrum of FA-LZM (e, f) and FAM-LZM (g, h). ($C_{LZM} = 1.58 \times 10^{-4}$ moL•L^{-1}, T = 297 K, C_{FA} (a-j) = C_{FAM}(a-j) = 7.50, 15.00, 22.50, 30.00, 37.50, 45.00, 52.50, 60.00, 67.50 ($\times 10^{-6}$ moL•L^{-1})).

in the polarity of the environment in which the amino acid residues were located, suggesting that the hydrophobicity of the microenvironment was reduced and the stretch degree of the peptide chain was enhanced. The maximum EM wavelength red shifted, indicating an increase in polarity when the amino acid residues were in a more "exposed" state, i.e., the protease structure became looser. The results from FAM-HSA, FA-LZM, and FAM-LZM were consistent with those from fluorescence quenching.

3.5. Three-dimensional (3D) fluorescence spectrum

3D fluorescence spectra can reveal the fluorescence characteristics of samples more directly and in detail, and improve the level of scientific research related to the determination of the conformational characteristics of proteins [46]. The 3D fluorescence spectrum of the interaction between FA and FAM with HSA and LZM is shown in Fig. 7. In the 3D fluorescence spectrum, peak 1 is Rayleigh scattering peak ($\lambda_{ex} = \lambda_{em}$); peak 2 is the overlapping fluorescence peak of Trp, Tyr, and Phe; and peak a is the second-order scattering peak. With the addition of FA and FAM, the intensities of peaks 1 and 2 of HSA and LZM decreased, and peak 2 underwent a blue shift, resulting in a decrease in the intensity of peak a of HSA. The reduction in Rayleigh scattering in Peak 1 indicated that the interaction with FA and FAM disrupts the surface protective layer of HSA and LZM, making the originally dispersed proteins more dispersed, reducing the particle size of the proteins, and reducing the Rayleigh scattering intensity of the 4 systems. The decrease in intensity of peak 2 and blue shift indicated that the microenvironment of the fluorescent group in LZM was slightly more nonpolar. The decrease in the intensity of peak 1 of the secondary structure indicated that the addition of FA and FAM led to changes in the peptide chain, leading to conformational changes in HSA and LZM [47].

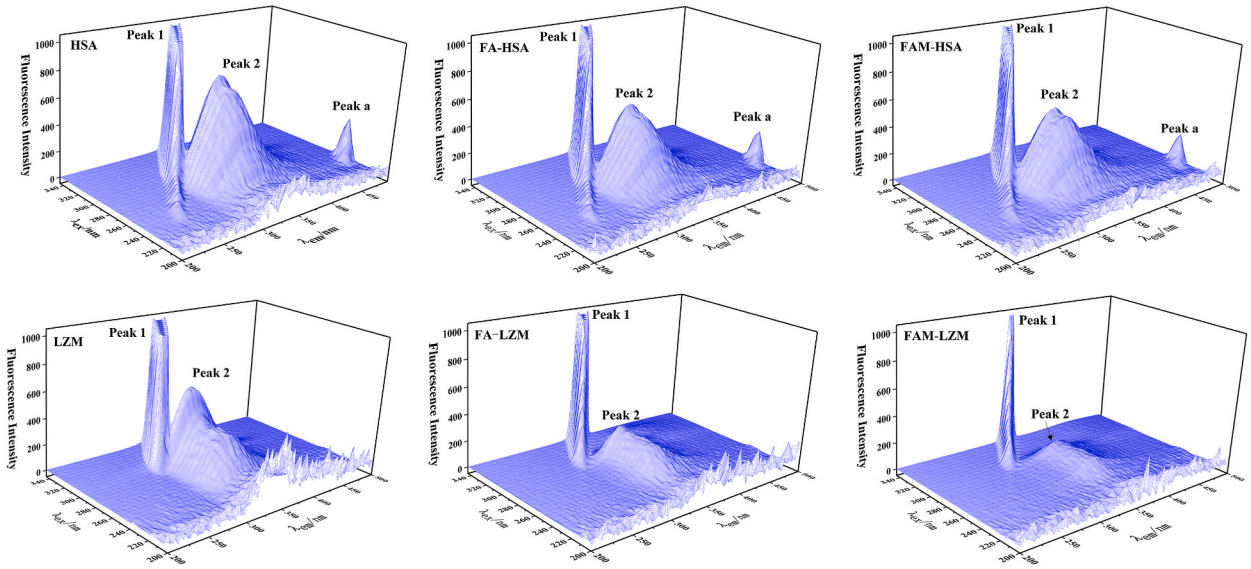

Fig. 7. Three-dimensional fluorescence spectrum of HSA, LZM, FA-HSA, FAM-HSA, FA-LZM, and FAM-LZM.

3.6. Circular dichroism

Circular dichroism (CD) is an effective technique to determine changes in protein structure [48–51]. It is now an important spectral method to study molecular configurations and intermolecular interactions. The measurement range of 180 nm–250 nm in the CD spectrum mainly reflects the α-helix, β-folding, and random coil of proteins [52]. The measurement results of α-helix, β-folding, and irregular curling in the 4 systems are shown in Table 4. When FA concentration in the solution increased, the α-helix concentration of HSA decreased from 62.4 % to 57.3 %, and that of LZM decreased from 92.8 % to 86.5 %. When the concentration of FAM increased, the α-helix concentration of HSA decreased from 62.4 % to 57.8 % and that of LZM decreased from 92.8 % to 87.7 %. The spectra of the secondary structures of HSA and LZM acquired using CD are shown in Fig. 8. The absorption intensity increased gradually with an increase in FA and FAM concentrations, indicating that the increase led to changes in the secondary structure of Trp [53]. The CD spectra showed no significant changes in the peak shape and position of the negative peak, indicating that after the combination reaction of FA and FAM with HSA and LZM, the helical structure became looser. Thus, the binding effect led to changes in the secondary structure of HSA and LZM, but the structure of α-helix was still dominant [54].

Table 4
The effect of FA and FAM on the secondary structure of HSA and LZM.

	Concentration of FA or FAM ($mol \bullet L^{-1}$)	α-Helix (%)	β-Sheet (%)	β-Turn (%)	Random coil (%)
FA-HSA	0.00	62.4	7.4	12.8	17.3
	1.25	60.0	7.9	13.1	18.4
	2.50	59.6	8.1	13.1	18.5
	3.75	58.6	8.3	13.3	19.0
	5.00	57.3	8.6	13.4	19.6
FAM-HSA	0.00	62.4	7.4	12.8	17.3
	1.25	64.5	7.0	12.5	16.4
	2.50	61.5	7.6	12.9	17.7
	3.75	59.8	7.9	13.1	18.5
	5.00	57.8	8.5	13.4	19.4
FA-LZM	0.00	92.8	1.8	7.9	4.5
	1.25	91.8	1.9	8.2	4.9
	2.50	90.6	2.2	8.5	5.5
	3.75	89.0	2.4	8.9	6.2
	6.25	86.5	2.8	9.4	7.2
FAM-LZM	0.00	92.8	1.8	7.9	4.5
	1.25	91.9	1.8	8.2	4.9
	2.50	90.9	2.0	8.4	5.3
	3.75	89.4	2.4	8.8	6.0
	5.00	87.7	2.6	9.1	6.7

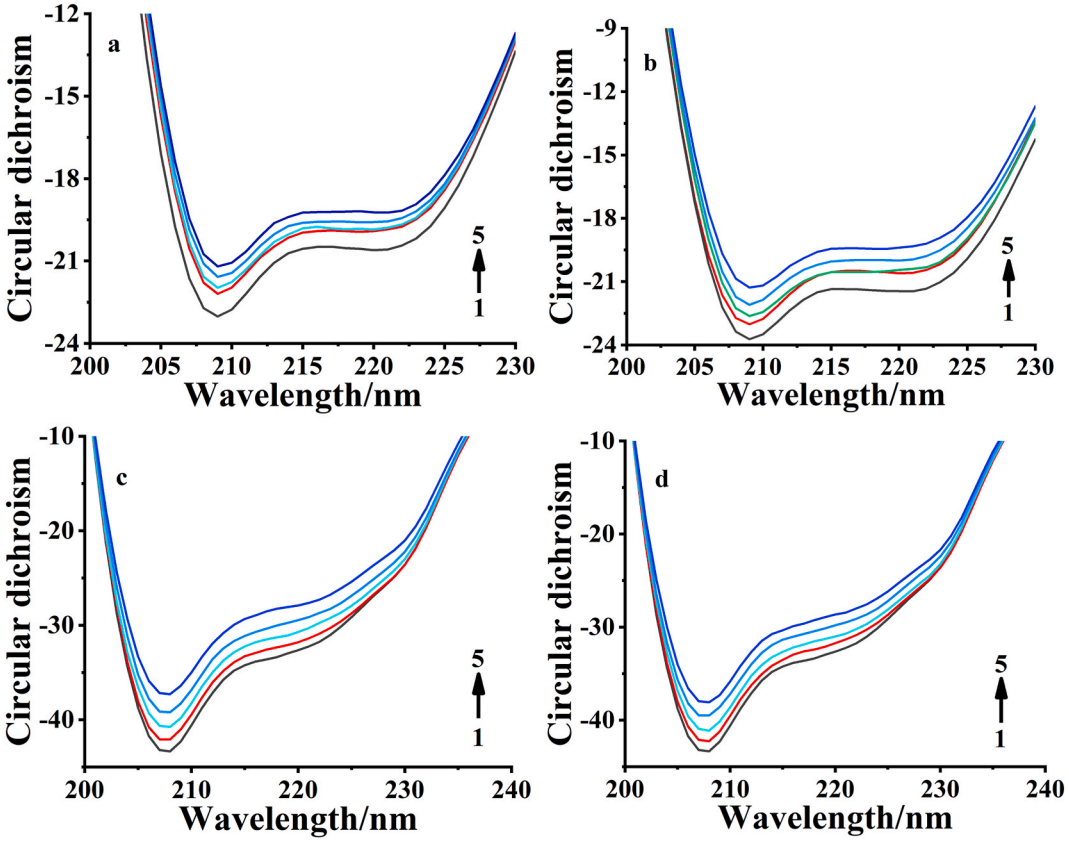

Fig. 8. Circular dichroism of FA-HSA(a) and FAM-HSA(b), (C_{FA} (1–5) = C_{FAM} (1–5) = 0.00, 1.25, 2.50, 3.75, 5.00 ($\times 10^{-4}$ mol L^{-1})). Circular dichroism of FA-LZM(c) and FAM-LZM(d), C_{FA} (1–5) = C_{FAM} (1–5) = 0.00, 0.40, 0.80, 1.20, 1.60 ($\times 10^{-6}$ mol L^{-1})).

3.7. Resonance light scattering

Resonant light scattering (RLS) is an analytical method based on the resonance of light scattering with molecular light absorption [55]. RLS in the range of 200 nm–700 nm was measured, and the results are shown in Fig. 9. Curve B shows the RLS spectrum of the blank solution with strong RLS signal intensity. As different concentrations of FA and FAM solutions were added, the RLS intensity of the system weakened. FA and FAM react with HSA and LZM, respectively, to form complexes, resulting in a decrease in the scattered light intensity of the system. This finding indicated that the HSA and LZM conformations underwent changes during the interaction process, resulting in a decrease in protein size and the extent of aggregation [56]. Our findings were consistent with the results from fluorescence experiments.

3.8. Molecular docking and molecular dynamics simulation

3.8.1. Molecular docking

Molecular docking gives us an in-depth understanding of the secondary connections of HSA and LZM molecules, the binding force types in structural change systems, and the interactions of FA and FAM with HSA and LZM, respectively [57–59]. The binding energy of small molecules and proteins is shown in Table 5.

In the FA-HSA system (Fig. 10a), FA formed a pi-pi stacked interaction with Tyr161 and Tyr138, a pi-sulfur interaction with Met 123, a pi-alkyl hydrophobic interaction with Leu 182, and mainly hydrogen bond interactions with Leu 135, Arg186, and Tyr161 of the amino acid residues of HSA. The results showed that the docking binding energy of the protein HSA and the small molecule FA was −7.6 kcal/mol.

In the FAM-HSA system (Fig. 10b), FAM formed a hydrogen bond with Val482, Leu481, Lys199; a pi-sigma interaction with TRP214, and mainly pi-alkyl hydrophobic interactions with Ala 210, Leu 347, Phe211, Leu481, Lys199, and Val482 of the amino acid residues of HSA. The results showed that the docking binding energy of the protein HSA and the small molecule FAM was −7.1 kcal/mol.

In the FA-LZM system (Fig. 10c), FA formed a pi-pi T-shaped interaction with TRP109 and a pi-alkyl hydrophobic interaction with Ala108 and Trp64, and mainly interacted with Ser 51 and Trp64 of the LZM amino acid residues to form hydrogen bonds. The results showed that the docking binding energy of the protein LZM and the small FA was −5.7 kcal/mol.

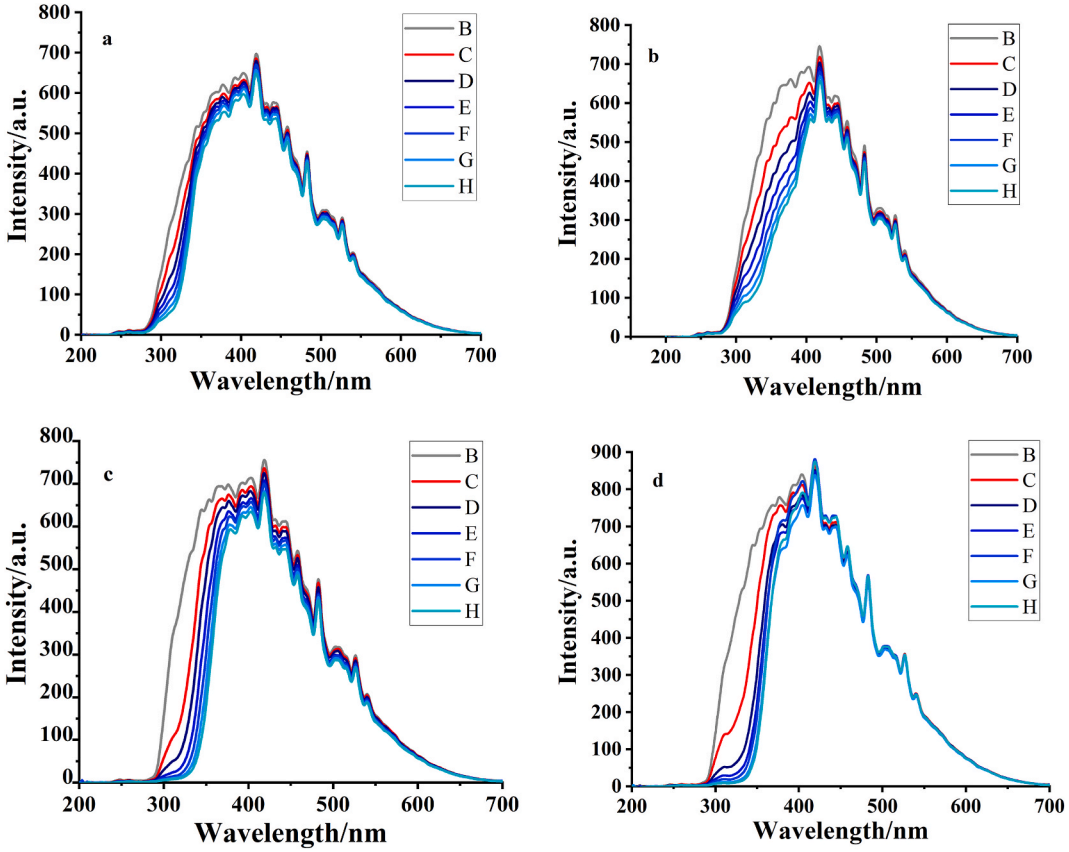

Fig. 9. Resonance light scattering spectrum of FA-HSA(a), FAM-HSA(b), FA-LZM(c) and FAM-LZM(d).

Table 5
Binding energy of FA-HSA, FAM-HSA, FA-LZM, and FAM-LZM.

Small Molecules	HSA	LZM
FAM	−7.1	−5.6
FA	−7.6	−5.7

In the FAM-LZM system (Fig. 10d), FAM formed a hydrogen bond interaction with Trp64 and Asn 46 and mainly formed a pi-alkyl hydrophobic interaction with Ala108, Trp109, and Val 99 of the amino acid residues of LZM. The results showed that the docking binding energy of protein LZM and the small molecule FAM was −5.6 kcal/mol.

The docking energy refers to the energy released by molecules in the process of mutual recognition and binding, which can reflect the interaction strength and bonding tightness between molecules [60]. It can be seen from the above results that the binding activity of FA to protein was stronger than that of FAM to protein, which may be related to the substituents. This is consistent with the binding constants of the four systems when the binding ability is the strongest. In addition, the interactions of FA and FAM with HSA and LZM were hydrophobic interactions and hydrogen bonding.

3.8.2. Molecular dynamics simulation

Using molecular dynamics (MD) based modeling methods, the adsorption situation of each force that led to the small molecule to bind to the protein was analyzed (Fig. 11). There are 3 homologous domains after FA and FAM combine with HSA, which are domains I, II, and III. The subdomain consists of IBA, IIA, IIA-IIB, IIIA, and IIIB. The small molecule FA binds to the active site of HSA. The aromatic ring center of FA interacts with Tyr138 near the active site. In addition, the oxygen atom of the methyl group on FA forms a hydrogen bond interaction with Arg186. The aromatic ring center of the small molecule FAM interacts with Phe211 of HSA, and the carbonyl and hydroxyl groups on FAM form hydrogen bond interactions with Val482 and Lys199. The aromatic ring center of FA can form interactions with Trp109 of LZM, and the methoxy group on it interacts with Trp64. The aromatic ring center of the small molecule FAM interacts with Trp109 of LZM, and the methoxy group on FAM interacts with Trp64. The structures of FA and FAM are similar and bind to the same sites of LZM and therefore have similar binding patterns.

The trajectory stability of RMSD reflects the strength of HSA, LZM, and the 4 compounds combined with FA and FAM in the solvent.

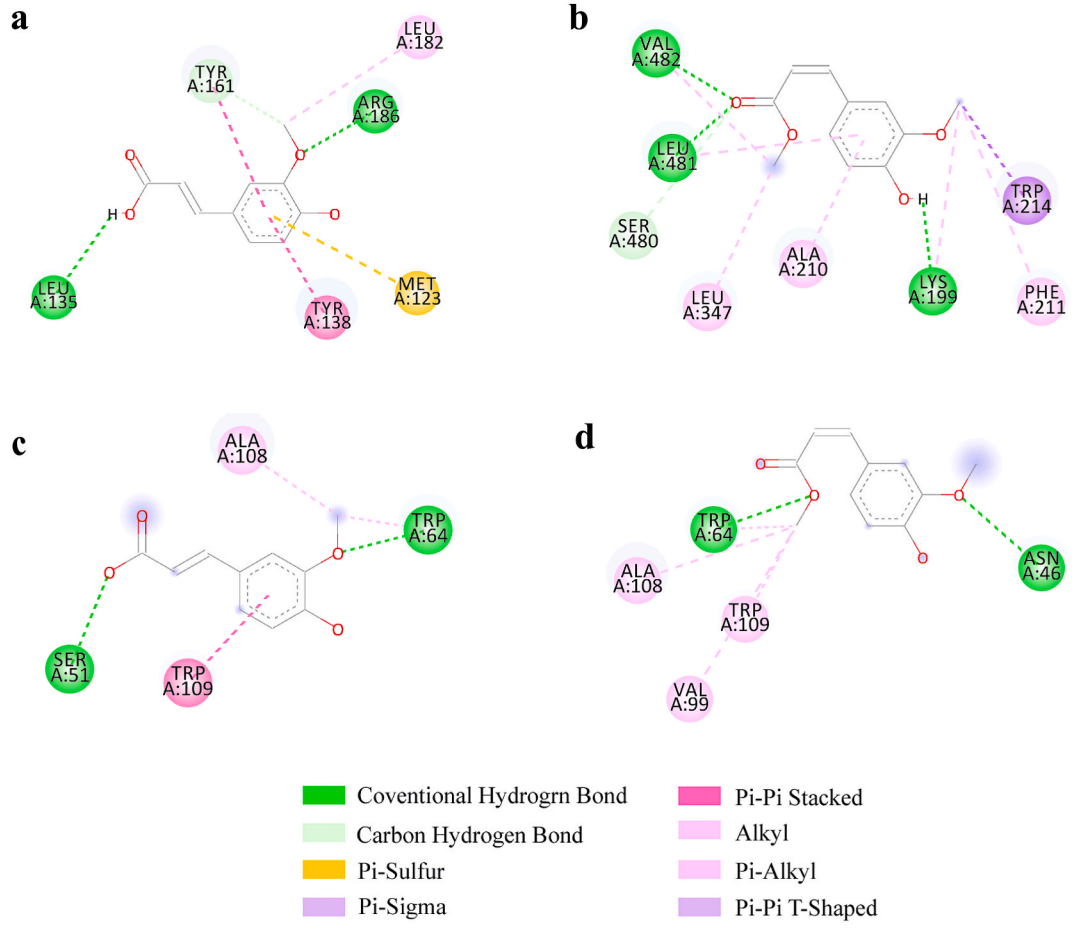

Fig. 10. Molecular docking of FA-HSA(a), FAM-HSA(b), FA-LZM(c), FAM-LZM(d) system.

The stable value in the trend of RMSD values also proves that the simulation system has reached equilibrium conditions [61]. As shown in Fig. 12a and b, at the initial stage of simulation, there was no significant change in HSA and LZM after binding with the small molecules. At the same time, FA-HSA, FAM-HSA, FA-LZM, and FAM-LZM did not change significantly. Compared with FA-HSA, the faster convergence and lower noise of RMSD values in the FAM-HSA system indicated higher and stronger interactions between HSA and FA. RMSD simulated by molecular dynamics of pure LZM protein fluctuated more than that of FA-LZM and FAM-LZM systems, indicating that the complexes formed by binding with FA and FAM were more stable. Moreover, the RMSD of the LZM-FAM system was similarly to that of LZM-FA.

RMSF can be used to determine the flexibility of fragments in each region of the protein structure [62]. The peaks and valleys of the RMSF curves of the 4 systems were similar, indicating that the protein structure was not mutated during simulation. RMSF simulated by molecular dynamics of pure HSA and LZM proteins fluctuated more, indicating that HSA and LZM were more stable after binding with FA and FAM. Additionally, the RMSF value of the FAM-HSA complex was lower than that of the FA-HSA complex, indicating that the stability of HSA increased after the combination of FAM and HSA. The RMSF values of the FAM-LZM complex were in phase with the RMSF of the FA-LZM complex, indicating that the stability of the protein after combining FA and FAM with LZM was similar. Owing to the rigidity of the residues involved in the binding of small molecules to proteins during simulation, the fluctuation curves of free proteins and complexes were similar [63].

The tightness of a protein is measured by the radius of rotation (R_g) [64] (Fig. 12e and f). The R_g values were almost constant, indicating that the FA-HSA, FAM-HSA, FA-LZM, and FAM-LZM complexes were stable and that the proteins were in a folded form during simulation at 298 K. The R_g values of the 4 systems were lower than those of pure HSA and LZM. This decrease in R_g value confirmed that the energy levels and stability of HSA and LZM were directly related to the combination of FA and FAM, and the adsorption of FA and FAM resulted in a decrease in the energy levels of HSA and LZM, thereby enhancing the stability of the proteins. In addition, the R_g value of FAM-HSA was lower than that of the FA-HSA system, indicating that FAM caused the conformation of HSA to become tightly compact.

The solvent-accessible surface area (SASA) is the surface area of biomolecules that is solvent accessible [65]. Fig. 12g and h shows the calculated SASA values for the 4 simulated systems. The SASA values for the FA-LZM and FAM-LZM systems were very close to each

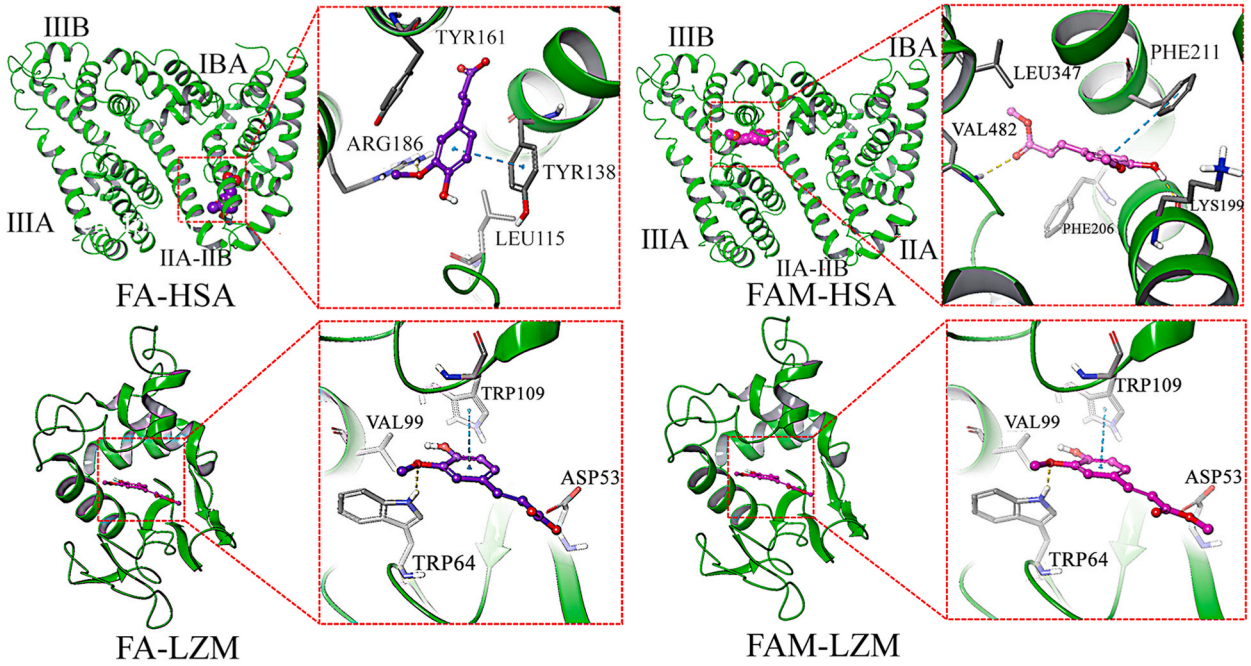

Fig. 11. The interactions between FA and FAM with HSA and LZM.

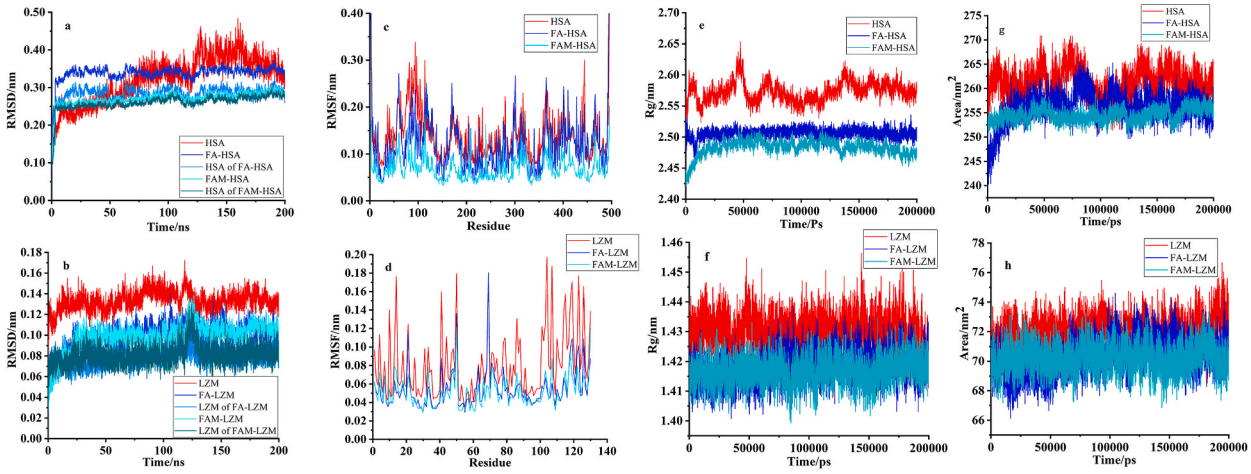

Fig. 12. Rmsd of FA and FAM with HSA(a), RMSD of FA and FAM with LZM(b), RMSF of FA and FAM with HSA(c), RMSF of FA and FAM with LZM (d), R_g of FA and FAM with HSA(e), R_g of FA and FAM with LZM(f), SASA of FA and FAM with HSA(g), SASA of FA and FAM with LZM(h).

other and almost stable over time. The SASA value of FAM-HSA was significantly higher than that of FA-HSA. These results are consistent with the values determined by the R_g value.

Results from hydrogen bond calculations validate the difference in the values of nonbonded interactions between small molecules and proteins (Fig. 13). In the early simulation stage of the FA-HSA system, small molecules and proteins did not form a stable complex, and the number of hydrogen bonds fluctuated between 0 and 1. When the simulation of the system was stable, the number of hydrogen bonds was stable at 1, which was consistent with the result of the *n* value in 3.3.1. The number of hydrogen bonds formed by FAM and HSA fluctuated between 1 and 2, and the effect intensity was greater than that of FA. At the later stage of the simulation of FA-LZM and FAM-LZM systems, the hydrogen bonds formed by FA, FAM, and LZM were basically stable at 1, which was consistent with the conclusion in Section 3.3.1.

Fig. 14 shows the structure of the complexes of the 4 systems. After FA and FAM were bound to the active site, HSA and LZM showed strong movement, indicating that binding had a greater effect on protein structure.

The contribution values of amino acid residues of HSA and LZM to binding energy are shown in Fig. 15. Tyr138 and Arg186 are involved in the binding to HSA near the active site of FA. Lys199, Phe211, and Val482 are involved in the bonding between FAM and

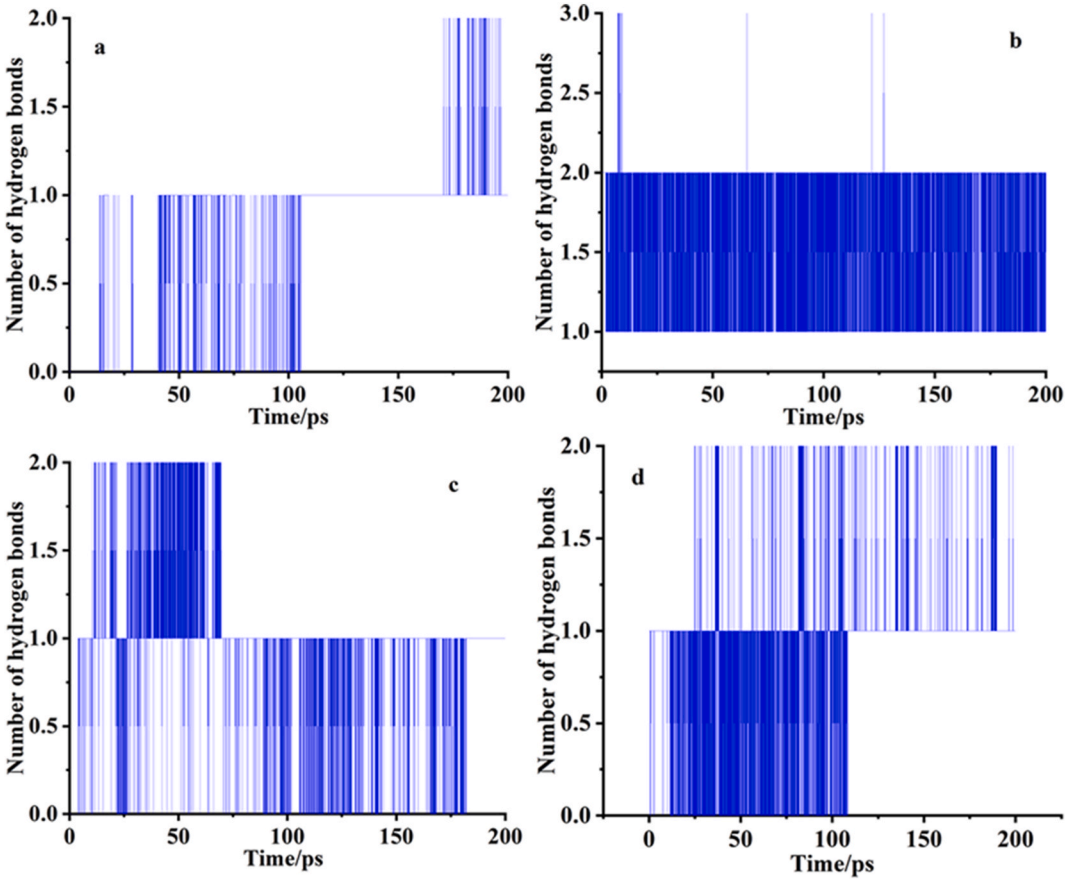

Fig. 13. Hydrogen bonds calculations of FA-HSA(a), FAM-HSA(b), FA-LZM(c) and FAM-LZM(d).

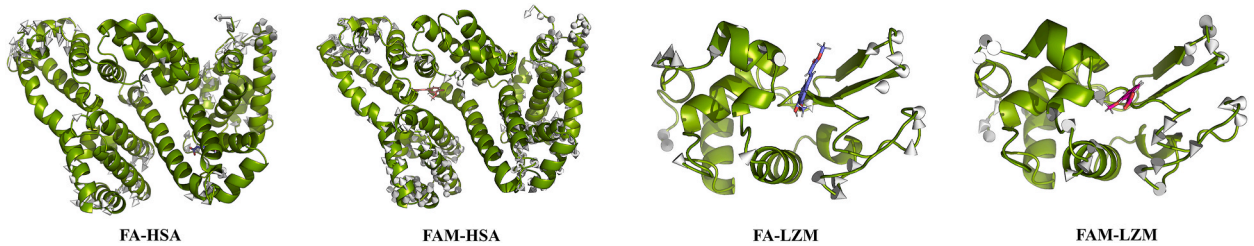

Fig. 14. The structure of the four system complexes.

HSA, whereas Trp64 and Trp109 are involved in the bonding between FA and LZM. Trp64 and Trp109 participated in the bonding between FAM and LZM. The amino acid residues of these proteins all promoted the binding of small molecules to proteins.

3.9. Effects of several metal ions on the binding constants

Human blood contains numerous common metal ions, and certain metal ions may affect the binding of small molecular substances to carriers in the human body [66]. This article studies the impact of K^+, Ca^{2+}, Cu^{2+}, Mg^{2+}, and Mn^{2+} on the binding strength of FA-HSA, FAM-HSA, FA-LZM, and FAM-LZM systems. Table 6 shows that at 294 K, in the FA-HSA system, the binding strength of the 5 metal ions with FA-HSA was K_a (Ca^{2+}) > K_a (Cu^{2+}) > K_a (K^+) > K_a (Mg^{2+}) > K_a (Mn^{2+}). The Ca^{2+} binding constant was the largest, indicating that it formed the most stable complex with FA-HSA. At the same temperature, the binding strength of several metal ions with FAM-HSA was K_a (K^+) > K_a (Ca^{2+}) > K_a (Mg^{2+}) > K_a (Cu^{2+}) > K_a (Mn^{2+}), and the binding constant of K^+ was the largest, which indicated that the formation of the complex with FAM-HSA was the most stable. The binding strength of several metal ions with FA-LZM was K_a (Ca^{2+}) > K_a (Mn^{2+}) > K_a (K^+) > K_a (Mg^{2+}) > K_a (Cu^{2+}), and the binding constant of Ca^{2+} was the largest, which indicated that the formation of the complex with FA-LZM was the most stable. In the FAM-LZM system, the metal ions reduced the

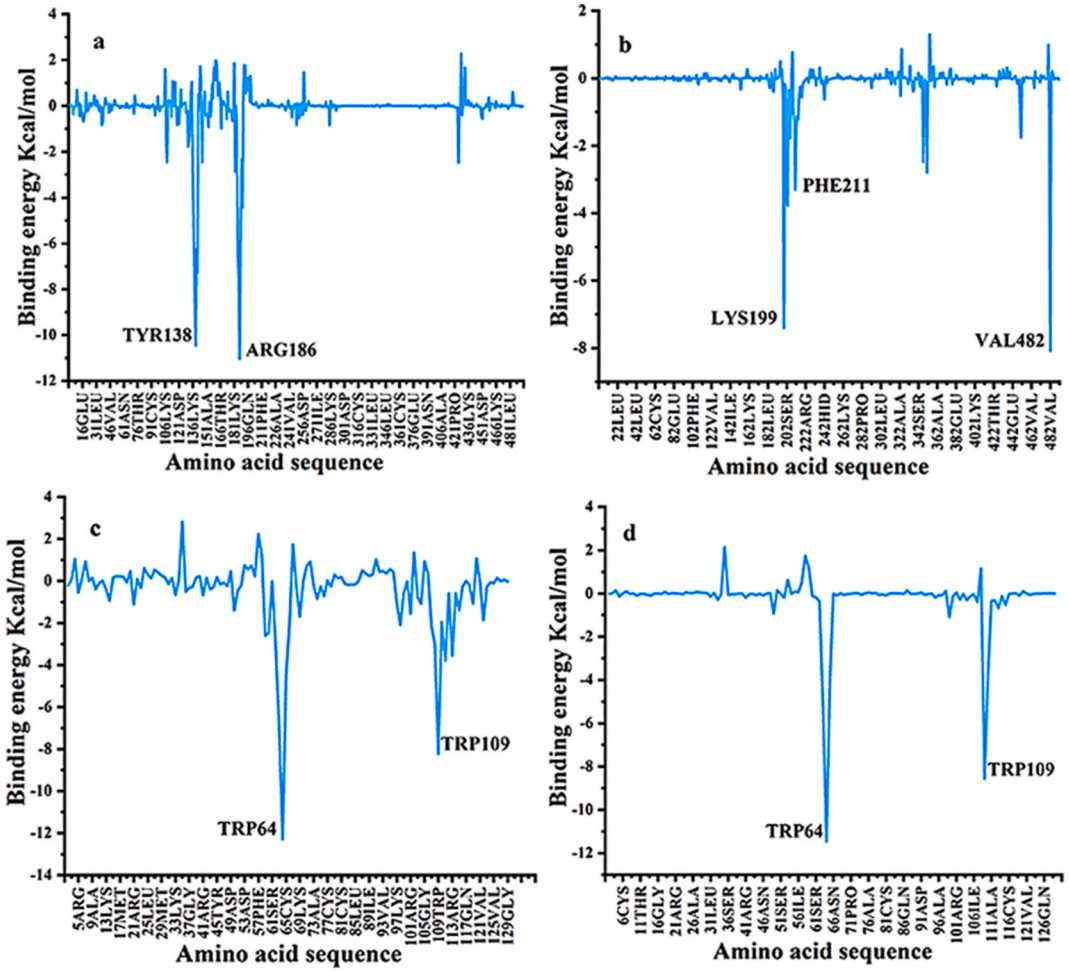

Fig. 15. Contribution of amino acid residues of HSA and LZM to binding energy.

Table 6
Several metal ions on the binding constants of FA-HSA, FAM-HSA, FA-LZM, FAM-LZM systems.

Substrate	Metal ion	K_a	
		FA	FAM
HSA	None	2.5668×10^4	8.2756×10^4
	K^+	4.5123×10^4	3.7325×10^5
	Ca^{2+}	7.4028×10^6	2.4689×10^5
	Cu^{2+}	6.6619×10^4	1.9143×10^5
	Mg^{2+}	4.2179×10^4	2.0281×10^5
	Mn^{2+}	3.9418×10^4	1.3341×10^5
LZM	None	5.7020×10^3	2.3280×10^4
	K^+	1.1649×10^4	2.2166×10^4
	Ca^{2+}	4.0290×10^6	9.2550×10^3
	Cu^{2+}	1.0205×10^4	1.2265×10^4
	Mg^{2+}	1.0957×10^4	1.8591×10^4
	Mn^{2+}	3.7523×10^4	2.0701×10^4

binding strength of the system, and Ca^{2+} had the greatest effect on FAM-LZM.

3.10. Effects of FA and FAM on the physiological functions of HSA and LZM

3.10.1. Determination of esterase activity

HSA and LZM have esterase-like activity and can hydrolyze pNPA to produce *p*-nitrophenol, which has maximum absorption at a

wavelength of 400 nm [67]. The effects of FA and FAM on HSA and LZM esterase activity can be obtained by measuring the absorbance changes of the products. As shown in Fig. 16, the esterase activity of HSA decreased slowly with an increase in FA and FAM concentrations. The esterase activity of LZM decreased with the increase in FA concentration but increased with the increase in FAM concentration. FAM has a significant impact on the esterase activity of LZM. The reason for the decrease in esterase activity was that the addition of FA and FAM increased the folding degree of proteins, and some hydrolyzable pNPA groups in their structures were no longer exposed to the protein surface, resulting in a decrease in the esterase activity of proteins. The research results from protein structure changes were used to analyze the reasons for the change in esterase activity [68]. During the process of FA and FAM acting on proteins leading to a change in the structure and the formation of a more stable structure of the protein itself, some groups that can hydrolyze pNPA were no longer exposed to the protein surface. As the number of groups decreased, the esterase activity of the protein decreased.

3.10.2. Radical-scavenging effect

The free cysteine in HSA and LZM plays an important role in scavenging free radicals [69]. Ellmann reagent reacts with free thiol groups to generate a yellow complex that has maximum absorption at 412 nm. By determining the changes in absorbance of the complex, the effects of FA and FAM on the ability of HSA and LZM to scavenge free radicals were determined. Fig. 17 shows the relationship between the contents of FA and FAM and the absorbance of the 4 systems. As the concentration of FA increased, the absorbance of HSA and LZM decreased slightly, indicating a decrease in the antioxidant capacities of HSA and LZM. The absorbance increased with an increase in FAM concentration, indicating an improvement in the antioxidant capacities of HSA and LZM. This may be because of the large changes in the protein structure caused by high concentrations of FA and FAM, which increased the contact opportunity between the free sulfhydryl groups and Ellman reagent.

4. Conclusions

The interactions between the phenolic acids FA and FAM with endogenous proteins HSA and LZM were studied using multispectral and molecular dynamics simulations. The quenching mechanism of FA and FAM on HSA and LZM fluorescence was found to be via a static quenching process. Binding effect analysis revealed a binding site in all 4 systems and indicated that the binding was spontaneous and that there was nonradiative energy transfer. In addition, the synchronous fluorescence spectrum, 3D fluorescence spectrum, and RLS spectrum showed that the conformations of HSA and LZM changed with the addition of FA and FAM. CD and molecular dynamics simulations further supported this conclusion. Molecular docking and thermodynamic parameters indicated that for the FA-HSA, FAM-HSA, and FA-LZM systems, the interactions between small molecules and proteins were mainly through hydrophobic interactions and hydrogen bond interactions, whereas for the FAM-LZM system, the interaction between the small molecule and protein was mainly through hydrophobic interactions, hydrogen bond interactions, and van der Waals forces. In addition, all observations for the FA and FAM on the active sites of HSA and LZM, including RMSD, RMSF, R_g, SASA, and regular hydrogen bonding number analysis, showed

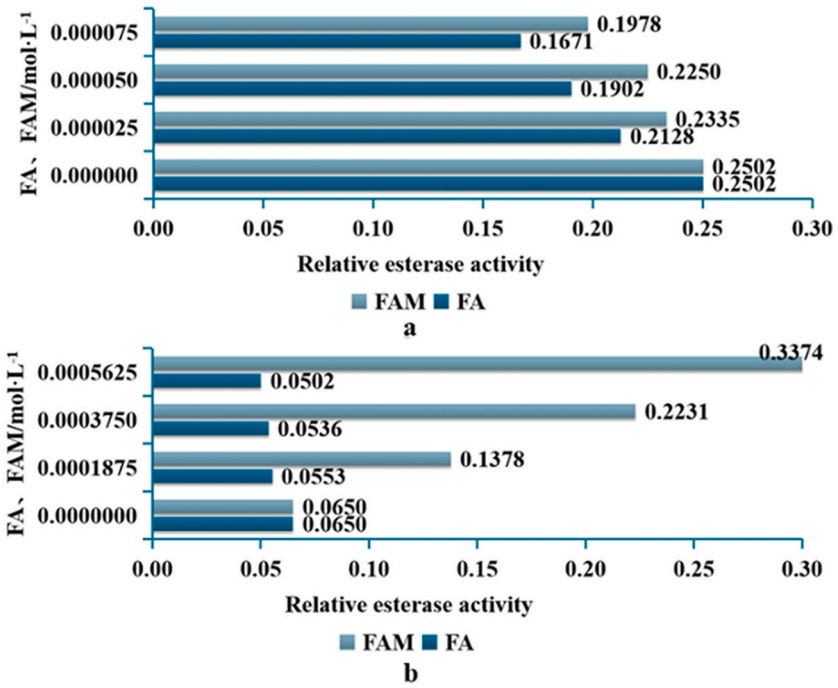

Fig. 16. Effects of FA and FAM on HSA esterase activity (a). Effects of FA and FAM on LZM esterase activity (b).

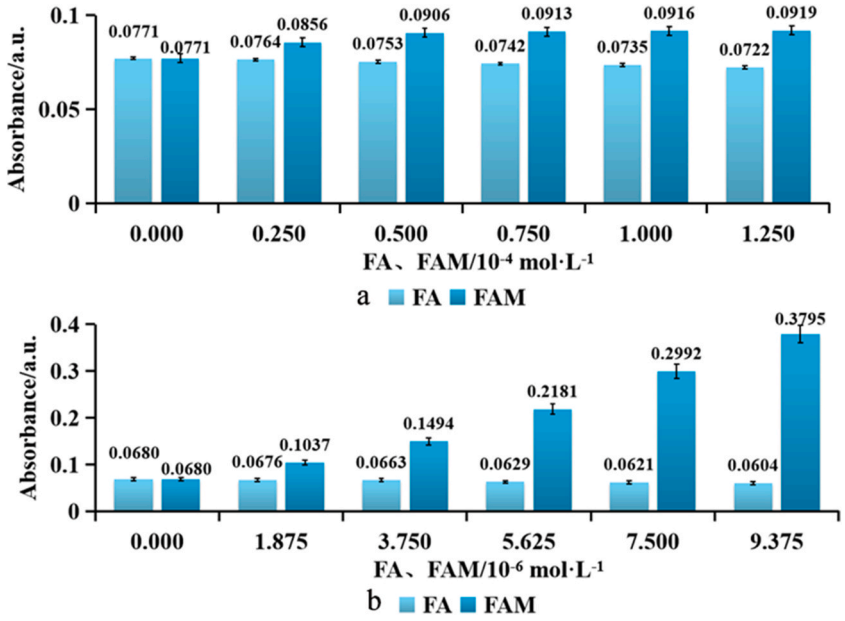

Fig. 17. The effect of FA and FAM on the scavenging ability of HSA free radicals(a). The effect of FA and FAM on the scavenging ability of LZM free radicals(b).

that proteins bound to small molecules were more stable than unbound proteins. In addition to the FAM-LZM system, the 6 metal ions resulted in tighter binding of proteins and small molecules in the FAM-LZM, FA-HSA, and FAM-HSA systems. Under the action of FA, the esterase activity of HSA and LZM decreased. Similarly, FAM also decreased the esterase activity of HSA. Meanwhile, the free radical-scavenging abilities of HSA and LZM were enhanced under the action of FAM. This study provides key data on the metabolism of phenolic acids in the human body, thereby highlighting important parameters of the health effects of such functional factors in foods. Meanwhile, the study of the interactions between the phenolic acids FA and FAM and endogenous proteins HSA and LZM is important for drug design and development as well as in food safety analysis. In the future, with more studies on the effects of phenolic acids and their derivatives on human endogenous proteins, it will promote the research and development of healthy foods and functional foods.

Data availability

Data will be made available on request.

Additional information

No additional information is available for this paper.

CRediT authorship contribution statement

Ying Yang: Formal analysis, Data curation, Conceptualization. **Shuqin Wang:** Methodology, Investigation. **Xingyan Liu:** Methodology. **Wenbin Zhang:** Software. **Wenhua Tong:** Writing – original draft. **Huibo Luo:** Supervision, Resources. **Liming Zhao:** Writing – review & editing.

Declaration of competing interest

The authors declare that they have no known competing financial interests or personal relationships that could have appeared to influence the work reported in this paper.

Acknowledgements

The Key Research and Development Project of Sichuan Provincial Science and Technology Department (NO.2022YFS0549), the Special Support of Sichuan Province 2022 Postdoctoral Research Project (NO.294074), Talent Introduction Project of Sichuan University of Science and Engineering (NO.2019RC31), the Graduate Innovation Fund of Sichuan University of Science and Engineering (NO.Y2022090, NO.Y2023247).

References

[1] N. Shinjyo, H. Fuchino, N. Kawahara, A. Hishida, Determination of (E)-ferulic acid content in the root of Angelica acutiloba: a simple chemical evaluation method for crude drug quality control, J. Nat. Med. 72 (3) (2018) 774–778.
[2] L. Liu, Y. Li, D. Lezhen, Y. Zhang, Z. Wua, J. Xiao, Reduction of Cardiovascular Disease Risks with Dietary Antioxidant Supplements, Dietary Supplements with Antioxidant Activity: Understanding Mechanisms and Potential Health Benefits: Dietary Supplements with Antioxidant Activity: Understanding Mechanisms and Potential Health Benefits 60 (2023).
[3] T. Masuda, K. Yamada, T. Maekawa, Y. Takeda, H. Yamaguchi, Antioxidant mechanism studies on ferulic acid: Isolation and structure identification of the main antioxidation product from methyl ferulate, Food Sci. Technol. Res. 12 (3) (2006) 173–177.
[4] Z. Wu, S. Yang, L. Xu, H. Li, J. Sun, Y. Xu, M. Huang, B. Sun, Screening and identifying microorganisms with feruloyl esterase activity in Chinese sesame-flavour baijiu fermentation materials (Jiupei), J. Food Compos. Anal. 102 (2021) 104069.
[5] S. Guo, X. Shi, F. Yang, L. Chen, E.J. Meehan, C. Bian, M. Huang, Structural basis of transport of lysophospholipids by human serum albumin, Biochem. J. 423 (1) (2009) 23–30.
[6] G. Rabbani, S.N. Ahn, Structure, enzymatic activities, glycation and therapeutic potential of human serum albumin: a natural cargo, Int. J. Biol. Macromol. 123 (2019) 979–990.
[7] G. Rabbani, S.N. Ahn, Review: Roles of human serum albumin in prediction, diagnoses and treatment of COVID-19, Int. J. Biol. Macromol. 193 (Pt A) (2021) 948–955.
[8] V. Arroyo, R. García-Martinez, X. Salvatella, Human serum albumin, systemic inflammation, and cirrhosis, J. Hepatol. 61 (2) (2014) 396–407.
[9] P. Dai, Q. Li, Research progress in the application of lysozyme in food and medicine field, in: E3S Web of Conferences, EDP Sciences, 2021 02048.
[10] W.H. Karasov, A.E. Douglas, Comparative digestive physiology, Compr. Physiol. 3 (2) (2013) 741.
[11] M. Hosseinzadeh, S. Nikjoo, N. Zare, D. Delavar, S. Beigoli, J. Chamani, Characterization of the structural changes of human serum albumin upon interaction with single-walled and multi-walled carbon nanotubes: spectroscopic and molecular modeling approaches, Res. Chem. Intermed. 45 (2019) 401–423.
[12] F. Kalhori, H. Yazdyani, F. Khademorezaeian, N. Hamzkanloo, P. Mokaberi, S. Hosseini, J. Chamani, Enzyme activity inhibition properties of new cellulose nanocrystals from Citrus medica L. pericarp: a perspective of cholesterol lowering, Luminescence 37 (11) (2022) 1836–1845.
[13] A. Sharifi-Rad, J. Mehrzad, M. Darroudi, M.R. Saberi, J. Chamani, Oil-in-water nanoemulsions comprising Berberine in olive oil: biological activities, binding mechanisms to human serum albumin or holo-transferrin and QMMD simulations, J. Biomol. Struct. Dyn. 39 (3) (2021) 1029–1043.
[14] H. Vahedian-Movahed, M. Saberi, J. Chamani, Comparison of binding interactions of lomefloxacin to serum albumin and serum transferrin by resonance light scattering and fluorescence quenching methods, J. Biomol. Struct. Dyn. 28 (4) (2011) 483–502.
[15] S. Khashkhashi-Moghadam, S. Soleimani, A. Bazanjani, S. Hoseinpoor, R. Taheri, P. Mokaberi, M.R. Saberi, J. Chamani, Fabrication of versatile and sustainable cellulose nanocrystals from lettuce stalks as potential tamoxifen delivery vehicles for breast cancer treatment: biophysical, cellular and theoretical studies, New J. Chem. 47 (31) (2023) 14768–14791.
[16] H. Maheri, F. Hashemzadeh, N. Shakibapour, E. Kamelniya, B. Malaekeh-Nikouei, P. Mokaberi, J. Chamani, Glucokinase activity enhancement by cellulose nanocrystals isolated from jujube seed: a novel perspective for type II diabetes mellitus treatment (In vitro), J. Mol. Struct. 1269 (2022) 133803.
[17] R. Taheri, N. Hamzkanlu, Y. Rezvani, S. Niroumand, F. Samandar, Z. Amiri-Tehranizadeh, M.R. Saberi, J. Chamani, Exploring the HSA/DNA/lung cancer cells binding behavior of p-Synephrine, a naturally occurring phenyl ethanol amine with anti-adipogenic activity: multi spectroscopic, molecular dynamic and cellular approaches, J. Mol. Liq. 368 (2022) 120826.
[18] W. Du, T. Teng, C.-C. Zhou, L. Xi, J.-Z. Wang, Spectroscopic studies on the interaction of bovine serum albumin with ginkgolic acid: binding characteristics and structural analysis, J. Lumin. 132 (5) (2012) 1207–1214.
[19] M. Chudzik, M. Maciążek-Jurczyk, B. Pawełczak, A. Sułkowska, Spectroscopic studies on the molecular ageing of serum albumin, Molecules 22 (1) (2016) 34.
[20] W. Tong, Y. Li, Z. Huang, S. Wang, G. Chen, X. Liu, Y. Yang, L. Zhao, Mechanism of molecular interaction between pyrazine flavor substances and Lysozyme: based on spectroscopy and molecular docking studies, J. Mol. Liq. 389 (2023) 122876.
[21] S. Huang, Q. Xiao, R. Li, H.-L. Guan, J. Liu, X.-R. Liu, Z.-K. He, Y. Liu, A simple and sensitive method for L-cysteine detection based on the fluorescence intensity increment of quantum dots, Anal. Chim. Acta 645 (1–2) (2009) 73–78.
[22] J. Minagawa, in: D. STERN, G. WITMAN (Eds.), Fluorescence Quenching Analysis, 2008.
[23] Z. Cheng, R. Liu, Spectroscopic studies on the interaction between tetrandrine and two serum albumins by chemometrics methods, Spectrochim. Acta Mol. Biomol. Spectrosc. 115 (2013) 92–105.
[24] M.H. Gehlen, The centenary of the Stern-Volmer equation of fluorescence quenching: from the single line plot to the SV quenching map, J. Photochem. Photobiol. C Photochem. Rev. 42 (2020) 100338.
[25] A. Jakubowska, EXPERIMENT 1 Determination of the Stern-Volmer Constant for Fluorescein Fluorescence Quenching..
[26] G. Rabbani, M.H. Baig, E.J. Lee, W.K. Cho, J.Y. Ma, I. Choi, Biophysical study on the interaction between eperisone Hydrochloride and human serum albumin using spectroscopic, calorimetric, and molecular docking analyses, Mol. Pharm. 14 (5) (2017) 1656–1665.
[27] M.S. Meaney, V.L. McGuffin, Investigation of common fluorophores for the detection of nitrated explosives by fluorescence quenching, Anal. Chim. Acta 610 (1) (2008) 57–67.
[28] N. Zhang, T. Zhang, X. Liu, G. Liu, J. Yan, K. Zheng, Corrigendum to “Speed tunability of the excited-state intramolecular proton transfer process based on seven-membered ring pyrrole-indole H-bond systems” [J. Mol. Liq. 286 (2019) 110887], J. Mol. Liq. 319 (2020) 114111.
[29] F. Urbina, K. Batra, K.J. Luebke, J.D. White, D. Matsiev, L.L. Olson, J.P. Malerich, M.A.Z. Hupcey, P.B. Madrid, S. Ekins, UV-adVISor: attention-based recurrent neural networks to predict UV-vis spectra, Anal. Chem. 93 (48) (2021) 16076–16085.
[30] A.P. Demchenko, Ultraviolet Spectroscopy of Proteins, Springer Science & Business Media, 2013.
[31] R. Li, L. Huang, Z. Zhang, J. Chen, H. Tang, Integrated multispectroscopic analysis and molecular docking analyses of the structure-affinity relationship and mechanism of the interaction of flavonoids with zein, Food Chem. 386 (2022) 132839.
[32] G. Rabbani, E.J. Lee, K. Ahmad, M.H. Baig, I. Choi, Binding of tolperisone hydrochloride with human serum albumin: effects on the conformation, thermodynamics, and activity of HSA, Mol. Pharm. 15 (4) (2018) 1445–1456.
[33] D. Genovese, M. Cingolani, E. Rampazzo, L. Prodi, N. Zaccheroni, Static quenching upon adduct formation: a treatment without shortcuts and approximations, Chem. Soc. Rev. 50 (15) (2021) 8414–8427.
[34] M.F. Dehkordi, S. Farhadian, F. Hashemi-Shahraki, B. Rahmani, S. Darzi, G. Dehghan, The interaction mechanism of candidone with calf thymus DNA: a multi-spectroscopic and MD simulation study, Int. J. Biol. Macromol. 235 (2023) 123713.
[35] S.R. Yazdi, M. Corredig, Heating of milk alters the binding of curcumin to casein micelles. A fluorescence spectroscopy study, Food Chem. 132 (3) (2012) 1143–1149.
[36] Z. Asemi-Esfahani, B. Shareghi, S. Farhadian, L. Momeni, Food additive dye–lysozyme complexation: determination of binding constants and binding sites by fluorescence spectroscopy and modeling methods, J. Mol. Liq. 363 (2022) 119749.
[37] Z. Malek-Esfandiari, A. Rezvani-Noghani, T. Sohrabi, P. Mokaberi, Z. Amiri-Tehranizadeh, J. Chamani, Molecular dynamics and multi-spectroscopic of the interaction behavior between bladder cancer cells and calf thymus DNA with rebeccamycin: apoptosis through the down regulation of PI3K/AKT signaling pathway, J. Fluoresc. 33 (4) (2023) 1537–1557.
[38] G. Rabbani, M.J. Khan, A. Ahmad, M.Y. Maskat, R.H. Khan, Effect of copper oxide nanoparticles on the conformation and activity of β-galactosidase, Colloids Surf. B Biointerfaces 123 (2014) 96–105.
[39] G.W. Gordon, G. Berry, X.H. Liang, B. Levine, B. Herman, Quantitative fluorescence resonance energy transfer measurements using fluorescence microscopy, Biophys. J. 74 (5) (1998) 2702–2713.
[40] B.A. Pollok, R. Heim, Using GFP in FRET-based applications, Trends Cell Biol. 9 (2) (1999) 57–60.

[41] J. Ma, J. Cao, Förster resonance energy transfer, absorption and emission spectra in multichromophoric systems. I. Full cumulant expansions and system-bath entanglement, J. Chem. Phys. 142 (9) (2015).
[42] X.-Y. Zhang, K. Wang, Y. Chang, X.-L. Hu, Z.-M. Su, E.-L. Zhou, Three Cd-MOFs with water stability act as novel fluorescent probes for detecting nitrofuran, nitrofurantoin and Fe3+, J. Solid State Chem. 313 (2022) 123170.
[43] J.R. Lakowicz, Principles of Fluorescence Spectroscopy, Springer, 2006.
[44] M. Guo, J.-W. Zou, P.-G. Yi, Z.-C. Shang, G.-X. Hu, Q.-S. Yu, Binding interaction of gatifloxacin with bovine serum albumin, Anal. Sci. 20 (3) (2004) 465–470.
[45] Y. Yang, Q. Wang, L. Lei, F. Li, J. Zhao, Y. Zhang, L. Li, Q. Wang, J. Ming, Molecular interaction of soybean glycinin and β-conglycinin with (−)-epigallocatechin gallate induced by pH changes, Food Hydrocolloids 108 (2020) 106010.
[46] L. Li, Y. Wang, W. Zhang, S. Yu, X. Wang, N. Gao, New advances in fluorescence excitation-emission matrix spectroscopy for the characterization of dissolved organic matter in drinking water treatment: a review, Chem. Eng. J. 381 (2020) 122676.
[47] B. Shen, H. Yang, J. Chen, X. Liu, M. Zhou, Study the interaction between juglone and calf thymus DNA by spectroscopic and molecular docking techniques, Spectrochim. Acta Mol. Biomol. Spectrosc. 261 (2021) 119998.
[48] G. Rabbani, E. Ahmad, N. Zaidi, R.H. Khan, pH-dependent conformational transitions in conalbumin (ovotransferrin), a metalloproteinase from hen egg white, Cell Biochem. Biophys. 61 (3) (2011) 551–560.
[49] G. Rabbani, E. Ahmad, N. Zaidi, S. Fatima, R.H. Khan, pH-Induced molten globule state of Rhizopus niveus lipase is more resistant against thermal and chemical denaturation than its native state, Cell Biochem. Biophys. 62 (3) (2012) 487–499.
[50] G. Rabbani, J. Kaur, E. Ahmad, R.H. Khan, S.K. Jain, Structural characteristics of thermostable immunogenic outer membrane protein from Salmonella enterica serovar Typhi, Appl. Microbiol. Biotechnol. 98 (6) (2014) 2533–2543.
[51] G. Rabbani, E. Ahmad, M.V. Khan, M.T. Ashraf, R. Bhat, R.H. Khan, Impact of structural stability of cold adapted Candida Antarctica lipase B (CaLB): in relation to pH, chemical and thermal denaturation, RSC Adv. 5 (26) (2015) 20115–20131.
[52] A. Gerbanowski, C. Malabat, C. Rabiller, J. Gueguen, Grafting of aliphatic and aromatic probes on rapeseed 2S and 12S proteins: influence on their structural and physicochemical properties, J. Agric. Food Chem. 47 (12) (1999) 5218–5226.
[53] A.I.A. Khayyat, S. Zargar, T.A. Wani, M.U. Rehman, A.A. Khan, Association mechanism and conformational changes in trypsin on its interaction with atrazine: a multi-spectroscopic and biochemical study with computational approach, Int. J. Mol. Sci. 23 (10) (2022) 5636.
[54] F. Li, B. Wang, B. Kong, S. Shi, X. Xia, Decreased gelling properties of protein in mirror carp (Cyprinus carpio) are due to protein aggregation and structure deterioration when subjected to freeze-thaw cycles, Food Hydrocolloids 97 (2019) 105223.
[55] R. Lan, W. Su, Y. Jia, J. Li, Simple and sensitive detection of persulfate based on a resonance light scattering spectroscopy, J. Water Chem. Technol. 44 (6) (2022) 482–487.
[56] L.R. Barbosa, M.G. Ortore, F. Spinozzi, P. Mariani, S. Bernstorff, R. Itri, The importance of protein-protein interactions on the pH-induced conformational changes of bovine serum albumin: a small-angle X-ray scattering study, Biophys. J. 98 (1) (2010) 147–157.
[57] E. Ahmad, G. Rabbani, N. Zaidi, S. Singh, M. Rehan, M.M. Khan, S.K. Rahman, Z. Quadri, M. Shadab, M.T. Ashraf, N. Subbarao, R. Bhat, R.H. Khan, Stereo-selectivity of human serum albumin to enantiomeric and isoelectronic pollutants dissected by spectroscopy, calorimetry and bioinformatics, PLoS One 6 (11) (2011) e26186.
[58] E. Ahmad, G. Rabbani, N. Zaidi, B. Ahmad, R.H. Khan, Pollutant-induced modulation in conformation and β-lactamase activity of human serum albumin, PLoS One 7 (6) (2012) e38372.
[59] A. Varshney, M. Rehan, N. Subbarao, G. Rabbani, R.H. Khan, Elimination of endogenous toxin, creatinine from blood plasma depends on albumin conformation: site specific uremic toxicity & impaired drug binding, PLoS One 6 (2) (2011) e17230.
[60] A.K. Bronowska, Thermodynamics of Ligand-Protein Interactions: Implications for Molecular Design, Thermodynamics-Interaction Studies-Solids, Liquids and Gases, IntechOpen, 2011.
[61] T. Savin, P.S. Doyle, Static and dynamic errors in particle tracking microrheology, Biophys. J. 88 (1) (2005) 623–638.
[62] G.R. Smith, M.J. Sternberg, P.A. Bates, The relationship between the flexibility of proteins and their conformational states on forming protein–protein complexes with an application to protein–protein docking, J. Mol. Biol. 347 (5) (2005) 1077–1101.
[63] M. Sahihi, G. Borhan, The effects of single-walled carbon nanotubes (SWCNTs) on the structure and function of human serum albumin (HSA): molecular docking and molecular dynamics simulation studies, Struct. Chem. 28 (2017) 1815–1822.
[64] L. Konermann, H. Metwally, R.G. McAllister, V. Popa, How to run molecular dynamics simulations on electrospray droplets and gas phase proteins: basic guidelines and selected applications, Methods 144 (2018) 104–112.
[65] S. Ausaf Ali, I. Hassan, A. Islam, F. Ahmad, A review of methods available to estimate solvent-accessible surface areas of soluble proteins in the folded and unfolded states, Curr. Protein Pept. Sci. 15 (5) (2014) 456–476.
[66] S.M.S. Abdullah, S. Fatma, G. Rabbani, J.M. Ashraf, A spectroscopic and molecular docking approach on the binding of tinzaparin sodium with human serum albumin, J. Mol. Struct. 1127 (2017) 283–288.
[67] M.S. Mafa, S. Malgas, B.I. Pletschke, Feruloyl esterase (FAE-1) sourced from a termite hindgut and GH10 xylanases synergy improves degradation of arabinoxylan, Amb. Express 11 (1) (2021) 1–9.
[68] G. Rabbani, M.H. Baig, A.T. Jan, E. Ju Lee, M.V. Khan, M. Zaman, A.E. Farouk, R.H. Khan, I. Choi, Binding of erucic acid with human serum albumin using a spectroscopic and molecular docking study, Int. J. Biol. Macromol. 105 (Pt 3) (2017) 1572–1580.
[69] P. Malik, T.K. Mukherjee, Immunological methods for the determination of AGE-RAGE axis generated glutathionylated and carbonylated proteins as oxidative stress markers, Methods 203 (2022) 354–363.